CERTIFICATE

This is to certify that The Thesis titled, **"Use of Micromechanical Modelling to assess the Fracture Characteristics of SS 304 Reactor grade steel"**, being submitted by **Ms. Shweta Miglani**, in partial fulfillment of the requirement for the award of degree of **MASTER OF ENGINEERING (CAD/CAM & ROBOTICS) at THAPAR UNIVERSITY, PATIALA** is a bonafide work carried out by her under our guidance and supervision and no part of this thesis has been submitted for the award of any other degree.

Mr. Rahul Chhibber
Lecturer
Mechanical Engineering Department.
Thapar University,
Patiala -147004

Dr. Bijan Kumar Dutta
Head,
Computational Mech. Section
Reactor Safety Division
BARC
Mumbai-400085

Dr S.K. Mohapatra
Professor & Head,
Thapar University,
Patiala -147004

Dr R.K. Sharma
Dean, Academic Affairs
Thapar University
Patiala-147004

ACKNOWLEDGEMENT

A dissertation cannot be completed without the help of many people who contribute directly or indirectly through there ceaseless and systematic assistance in the evolution and preparation of this work. A special debt of gratitude is owed to my thesis supervisor, ***Mr Rahul Chhibber lecturer, Mechanical Engineering Department, Thapar university, Patiala*** *and co supervisor,* ***Dr B.K, Dutta, Head, Computational Mechanics Section, BARC Mumbai*** *for his gracious efforts and stimulating support, which acted as a blessing for the successful fulfillment of my thesis. There Meticulous and conscientious enthusiasm has been highly beneficial in keeping my spirits high.*

I would also like to thank Mr. subhasish guin Scientific officer 'D' , BARC Mumbai for his valuable assistance and cooperation in providing me all the necessary inputs.

I feel very much obliged to ***Dr. S.K Mohapatra,*** *Professor & Head, Department of Mechanical Engg. and* ***Dr. Abhijit Mukherjee, Director, Thapar University*** *for their encouragement and inspiration for our visit to BARC, Mumbai I would also like to offer my sincere thanks to all faculty, teaching and non-teaching, of Mechanical Engg. Deptt., (MED), and staff of central library, TU, Patiala for there assistance.*

I am also thankful to the authors whose works I have consulted and quoted in this work. Last, but not least, very special thanks to my parents and my friends for their constant encouragement and best wishes. Their patience and understanding without which this study would not have been in this present form, is greatly appreciated.

Date: *SHWETA MIGLANI*
80681021

ABSTRACT

The primary heat transport (PHT) piping of any nuclear reactor is a critical system. Any failure of this system will lead to very grace consequences, not speaking of huge monetary losses resulting from non utilization of the reactor setup. Hence, it is necessary to have an accurate and reliable method of predicting the fracture behviour in such components.

Fracture resistance of a ductile material is conventionally characterized by J-Resistance curves. The original idea was that a unique fracture resistance curve would suffice to characterize the material .However testing of different specimens revealed considerable J_R curves due to different levels of triaxility imposed on the specimens. This raises the question of transferring fracture parameters from specimen to component level.

Under such circumstances it is advisable to use damage mechanics (micro mechanical analysis) the difficulty of geometry independency is largely overcome by the damage mechanics, which model the drop in load carrying capacity of a material with the increase in plastic strain such modeling is done considering nucleation, growth and coalescence of the voids in a material following large scale plasticity. There are a wide variety of techniques available in damage mechanics of them, gurson modal is one of the most powerful models and used successfully by researchers throughout the world. In this model the model parameters are determined using a hybrid methodology of metallographic study, different tensile test subsequent numerical Analysis and curve fitting and finally prediction of components fracture behaviour and comparison of the analytical and experimental results.

CONTENTS

LIST OF FIGURES

List of Tables

Nomenclature

Symbol	Abbreviations
a	Crack length
A	Crack-face area, constant
A_2	Constraint indexing parameter
A_i	Area of inclusion and void
A_T	Total area under observation
A_V	Area fraction of voids
b	Ligament length of specimen
B	Specific width, constant
CTOD	Crack tip opening displacement
CMOD	Crack mouth opening displacement
D	Damage parameter/Diameter
ΔD	Contraction in diameter
E	Young's Modulus
E_t	Tangent modulus of stress- strain
f	Void volume fraction
f_o	Initial void volume fraction
f_c	Critical void volume fraction
f_f	Final void volume fraction
f_n	Void volume fraction at saturated nucleation
f	Void increment rate

f	Modified void volume fraction
f_u	Modified ultimate void volume fraction
f_{growth}	Void growth rate
$f_{nucleation}$	Void nucleation rate
g_{kj}	Metric tensor
G	Crack extention rate
G_c	Elastic energy release rate
I_n	Integration constant
J	J-integral
K	Acceleration factor
K_I	Stress intensity factor
K_{IC}	Plane stress fracture toughness
L_T	Length observed by the microscope

CHAPTER 1

INTRODUCTION

1.1 HISTORY OF NUCLEAR ENERGY

It is human nature to test, to observe, and to dream. The history of nuclear energy is the Story of a centuries-old dream becoming a reality. Ancient Greek philosophers first developed the Idea that all matter is composed of invisible particles called atoms. The word 'ATOM' comes from the Greek word, atomos, meaning indivisible. Scientists in the 18th and 19th centuries revised the concept based on their experiments. By 1900, physicists knew that the atom contains large quantities of energy. British physicist Ernest Rutherford was called the father of nuclear science because of his contribution to the theory of atomic structure. In 1904 he wrote:

"If it were ever possible to control at will the rate of disintegration of the radio elements, an enormous amount of energy could be obtained from a small amount of matter".

Albert Einstein developed his theory of the relationship between mass and energy one year later. The mathematical formula is E= $(mc)^2$, or "energy equals mass times the speed of light Squared." It took almost 35 years for someone to prove Einstein's theory.

1.2 POWER OBTAINED FROM NUCLEAR POWER

Atomic energy has got a definite and decisive role to perform in the Indian power generation and supply sector. India being a developing country , a major share of India's overall electricity requirement has to be from non conventional resources as the conventional resources has got limitations to meet the galloping needs . India has achieved self sufficiency in the nuclear science and technology. Thanks to the pioneer efforts initiated by Dr. Homi bhabha who visualized the Indian nuclear program which has been meticulously carried on by the dedicated scientists and engineers of DAE family.

An adequate and uninterrupted power generation is an intrinsic essentiality for the overall development of any nation. In quantitative terms, the per capita consumption of electric energy is regarded as an indicative parameter of the socio economic growth rate of a nation.

The major contribution to India's power production programme comes from

- Coal based thermal power stations (58,000 MW in 2002, ~ 67% of total power output)
- Hydroelectric power generation
- Non - conventional sources (Nuclear, wind, tidal etc.)

Per capita power consumption in India is around 400 Kwh/yr, which is much below the world average consumption of 2400 Kwh/yr. Thus, massive increase in the power generation to match the world average consumption is needed in the coming years to enhance the overall national growth rate.

The Department of Atomic Energy (DAE) has been promoting nuclear power as the "obvious choice for India to solve its energy problems in the long-term" .Such promises that nuclear power would play an important role in satisfying India's energy needs have been routinely offered since the 1950s, but the actual growth of nuclear power in the country has been extremely modest. As of January 2005, the total installed nuclear power generation capacity is 2,770 MW, less than 3 per cent of the total installed electricity generation capacity in the country.

The promise offered by DAE is not only that nuclear power would form an important component of India's electricity supply, but that it would be cheap. As early as 1958, barely a few years after the DAE was set up, Homi Bhabha, the chief architect of the programme, projected "the contribution of atomic energy to the power production in India during the next 10 to 15 years" and concluded that "the costs of nuclear power would compare very favorably with the cost of power from conventional sources in many areas". The 'many areas' referred to regions that were remote from coalfields. In the 1980s the DAE stated that the cost of nuclear power "compares quite favorably with coal fired stations located 800 km away from the pithead and in the 1990s would be even cheaper than coal fired stations at pithead" . This projection was not fulfilled. A more recent Nuclear Power Corporation (NPC) internal study comes to the less optimistic conclusion that the "cost of nuclear electricity generation in India remains competitive with thermal (electricity) for plants located about 1,200 km away from coal pit head, when full credit is given to long-term operating cost especially in respect of fuel prices". Despite its inability to live up to its promises, the DAE has always received high levels of financial support from the government, which have increased over the last few years. This government support has once again revived the hopes of the DAE for large-scale expansion; the DAE envisions having a total installed capacity of 20,000 MW of nuclear power by the year 2020. The largest component of this would be in the form of Pressurised Heavy Water Reactors (PHWR).

This anticipated increase in nuclear power capacity, in particular the focus on PHWRs, makes an assessment of the economics of electricity generation in these reactors particularly relevant and urgent. Over a decade ago, a comparison of energy technologies had concluded that other options like coal and hydroelectric power were cheaper than nuclear power under realistic assumptions and "even if the projections and scenarios indicate large demand-supply gaps in the future, the most expensive way of bridging these gaps is through nuclear power plants"

1.3 NUCLEAR REACTOR

1.3.1 What Is A Nuclear Reactor?

All nuclear reactors are devices designed to maintain a chain reaction producing a steady flow of neutrons generated by the fission of heavy nuclei. They are, however, differentiated either by their purpose or by their design features. In terms of purpose, they are either research reactors or power reactors.

Research reactors are operated at universities and research centre in many countries, including some where no nuclear power reactors are operated. These reactors generate neutrons for multiple purposes, including producing radiopharmaceuticals for medical diagnosis and therapy, testing materials and conducting basic research.

Power reactors are usually found in nuclear power plants. Dedicated to generating heat mainly for electricity production, they are operated in more than 30 countries. Their lesser uses are drinking water or district water production. In the form of smaller units, they also power ships.

A nuclear reactor is a system that contains and controls sustained nuclear chain reactions. Reactors are used for generating electricity, producing radionuclide (for industry and medicine), conducting research, and military purposes. All of the various designs of power-producing reactors accomplish the same simple task: spinning a generator. Many commercial reactors pass water over heat-producing fuel rods to generate steam and run a turbine. Some designs call for the passage of helium over a pile of heat-producing fuel pebbles. Yet another design uses liquid sodium as a coolant.

1.3.2 Components of Nuclear Reactors

Main components

- **The core** of the reactor contains all of the nuclear fuel and generates all of the heat. It contains low-enriched uranium (<5% U-235), control systems, and structural materials. The core can contain hundreds of thousands of individual fuel pins.
- **The coolant** is the material that passes through the core, transferring the heat from the fuel to a turbine. It could be water, heavy-water, liquid sodium, helium, or something else. In the US fleet of power reactors, water is the standard.
- **The turbine** transfers the heat from the coolant to electricity, just like in a fossil-fuel plant.
- **The containment** is the structure that separates the reactor from the environment. These are usually dome-shaped, made of high-density, steel-reinforced concrete.
- **Cooling towers** are needed by some plants to dump the excess heat that can not be converted to energy due to the laws of thermodynamics. These are the hyperbolic icons of nuclear energy. They emit only clean water vapor.

Differentiating nuclear reactors according to their design features is especially pertinent when referring to nuclear power reactors (see Types of Nuclear Power Reactors).

There are many different types of power reactors. What is common to them all is that they produce thermal energy that can be used for its own sake or converted into mechanical energy and ultimately, in the vast majority of cases, into electrical energy.

In these reactors, the fission of heavy atomic nuclei, the most common of which is uranium-235, produces heat that is transferred to a fluid which acts as a coolant. During the fission process, bond energy is released and this first becomes noticeable as the kinetic energy of the fission products generated and that of the neutrons being released. Since these particles undergo intense deceleration in the solid nuclear fuel, the kinetic energy turns into heat energy.

In the case of reactors designed to generate electricity, to which the explanations below will now be restricted, the heated fluid can be gas, water or a liquid metal. The heat stored by the fluid is then used either directly (in the case of gas) or indirectly (in the case of water and liquid metals) to generate steam. The heated gas or the steam is then fed into the turbine driving an alternator.

Since, according to the laws of nature, heat cannot fully be converted into another form of energy, some of the heat is residual and is released into the environment. Releasing is either direct – e.g. into a river – or indirect, into the atmosphere via cooling towers. This practice is common to all thermal plants and is by no means limited to nuclear reactors which are only one type of thermal plant.

1.3.3 Types of Nuclear Reactor

Nuclear power reactors can be classified according to the type of fuel they use to generate heat.

Uranium–fuelled Reactors

The only natural element currently used for nuclear fission in reactors is uranium. Natural uranium is a highly energetic substance: one kilogram of it can generate as much energy as 10 tonnes of oil. Naturally occurring uranium comprises, almost entirely, two isotopes: U_{238} (99.283%) and U_{235} (0.711%). The former is not fissionable while the latter can be fissioned by thermal (i.e. slow) neutrons. As the neutrons emitted in a fission reaction are fast, reactors using U_{235} as fuel must have a means of slowing down these neutrons before they escape from the fuel. This function is performed by what is called a moderator, which, in the case of certain reactors (see table of **Reactor Types** below) simultaneously acts as a coolant. It is common practice to classify power reactors according to the nature of the coolant and the moderator plus, as the need may arise, other design characteristics.

REACTOR TYPE	**COOLANT**	**MODERATOR**	**FUEL**
Pressurised water reactors (PWR, VVER)	Light water	Light water	Enriched uranium
Boiling water reactors (BWR)	Light water	Light water	Enriched uranium
Pressurised heavy water reactor (PHWR)	Heavy water	Heavy water	Natural uranium
Gas-cooled reactors (Magnox, AGR, UNGG)	CO2	Graphite	Natural or enriched uranium
Light water graphite reactors (RBMK)	Pressurised boiling water	Graphite	Enriched uranium

Table 1.1 Types of nuclear reactor

PWRs and BWRs are the most commonly operated reactors in Organization for Economic Cooperation and Development (OECD) countries. VVERs, designed in the former Soviet Union, are based on the same principles as PWRs. They use “light water”, i.e. regular water (H_2O) as opposed to “heavy water” (deuterium oxide D_2O). Moderation provided by light water is not sufficiently effective to permit the use of natural uranium. The fuel must be slightly enriched in U_{235} to make up for the losses of neutrons occurring during the chain reaction. On the other hand, heavy water is such an effective moderator that the chain reaction can be sustained without having to enrich the uranium. This combination of natural uranium and heavy water is used in PHWRs, which are found in a number of countries, including Canada, Korea, Romania and India.

Graphite-moderated, gas-cooled reactors, formerly operated in France and still operated in Great Britain, are not built any more in spite of some advantages.

RBMK-reactors (pressure-tube boiling-water reactors), which are cooled with light water and moderated with graphite, are now less commonly operated in some former Soviet Union bloc countries. Following the Chernobyl accident (26 April 1986) the construction of this reactor type ceased. The operating period of those units still in operation will be shortened.

1.3.3.1 Pressurised Water Reactors

The fission zone (fuel elements) is contained in a reactor pressure vessel under a pressure of 150 to 160 bar (15 to 16 MPa). The primary circuit connects the reactor pressure vessel to heat exchangers. The secondary side of these heat exchangers is at a pressure of about 60 bar (6 MPa) - low enough to allow the secondary water to boil. The heat exchangers are, therefore, actually steam generators. Via the secondary circuit, the steam is routed to a turbine driving an alternator. The steam coming out of the turbine is converted back into water by a condenser after having delivered a large amount of its energy to the turbine. It then returns to the steam generator. As the water driving the turbine (secondary circuit) is physically separated from the water used as reactor coolant (primary circuit), the turbine-alternator set can be housed in a turbine hall outside the reactor building.

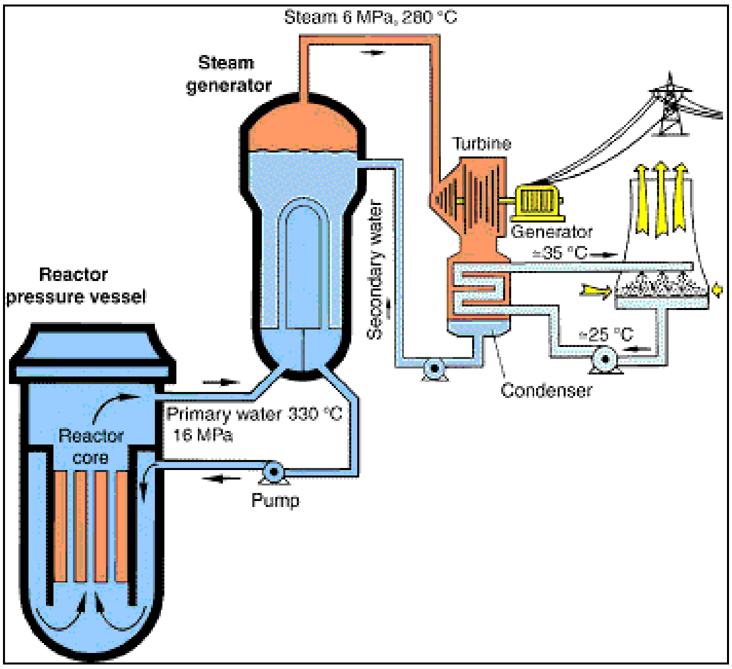

Figure 1.1: Nuclear power plant with pressurized water reactor

1.3.3.2 Boiling Water Reactors

The fission zone is contained in a reactor pressure vessel, at a pressure of about 70 bar (7 MPa). At the temperature reached (290 °C approximately), the water starts boiling and the resulting steam is produced directly in the reactor pressure vessel. After the separation of steam and water in the upper part of the reactor pressure vessel, the steam is routed directly to a turbine driving an alternator.

The steam coming out of the turbine is converted back into water by a condenser after having delivered a large amount of its energy to the turbine. It is then fed back into the primary cooling circuit where it absorbs new heat in the fission zone.

Since the steam produced in the fission zone is slightly radioactive, mainly due to short-lived activation products, the turbine is housed in the same reinforced building as the reactor.

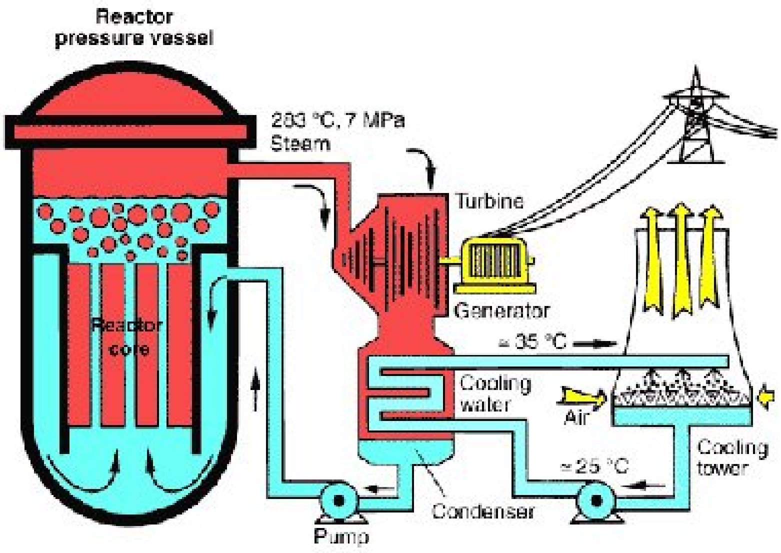

Figure 1.2: Principle of a nuclear power plant with boiling water reactor

For our purpose we will concentrate on Pressurised Heavy Water Reactor & Advanced Heavy Water Reactor and its Heat Transport system.

1.3.3.3 Pressurised Heavy Water Reactor

A pressurised heavy water reactor (PHWR) is a Nuclear Power reactor that uses unenriched natural uranium as its fuel and heavy water as its moderator (deuterium oxide D_2O). The heavy water is kept under pressure in order to raise its boiling point, allowing it to be heated to higher temperatures and thereby carry more heat out of the reactor core. While heavy water is expensive, the reactor can operate without expensive fuel enrichment facilities thus balancing the costs.

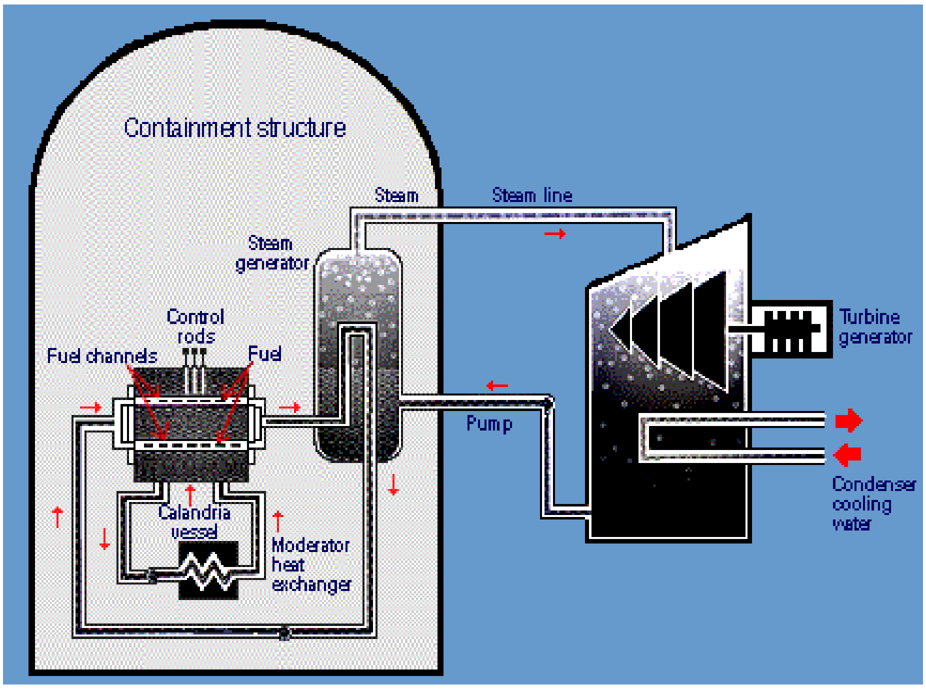

Figure 1.3: Pressurized heavy water reactor

1.3.3.4 Advanced Heavy Water Reactor

The Advanced Heavy Water Reactor (AHWR) is a proposed heavy water moderated nuclear power reactor that will be the next generation design of the PHWR type. It is now being developed at **Bhabha Atomic Research Centre** (BARC) and aims to meet the objectives of using thorium fuel cycles for commercial power generation. The AHWR is a vertical pressure tube type reactor cooled by boiling light water under natural circulation. A unique feature of this design is a large tank of water on top of the primary containment vessel, called the Gravity Driven Water Pool (GDWP). This reservoir is designed to perform several passive safety functions, these include: Core heat removal through natural circulation; direct injection of Emergency Core Coolant System (ECCS) water in fuel; and the availability of a large inventory of borated water in overhead Gravity Driven Water Pool (GDWP) to facilitate sustenance of core decay heat removal. The Emergency Core Cooling System (ECCS) injection and containment cooling can act without invoking any active systems or operator action.

The reactor design incorporates advanced technologies, together with several proven positive features of Indian Pressurised Heavy Water Reactors (PHWRs). These features include pressure tube type design, low pressure moderator, on-power refueling, diverse fast acting shut-down systems, and availability of a large low temperature heat sink around the reactor core.

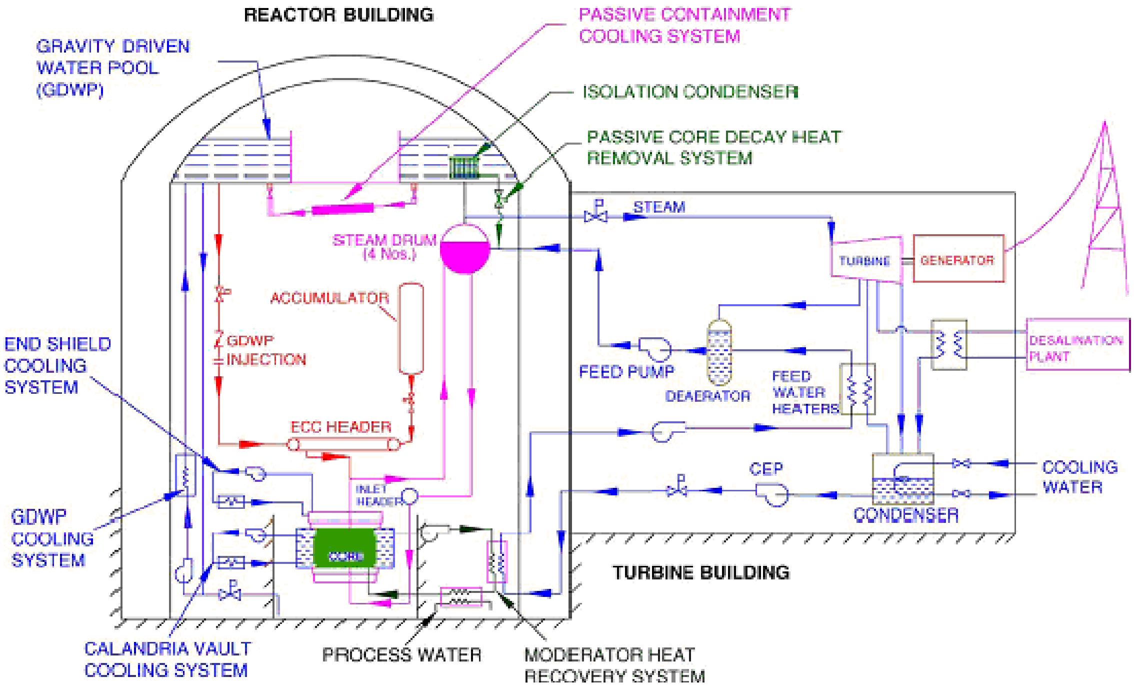

Figure 1.4: Advanced heavy water reactor

Rational for selection of PHWR for India's current Nuclear Power Plants program

The choice of PHWR in the current stage of India's Nuclear Power Plants program is based on the long-term objectives and availability of resources and infrastructure. Self-reliance and energy security have been among the important objectives of the Indian Nuclear Power Program right from its inception. This, together with the existence of modest resources of uranium and vast resources of thorium in the country led to the adoption of the three stage program (thermal reactors—plutonium-based fast breeders—^{233}U/thorium-based breeders) and choice of PHWR for the first stage of the program.

The features of PHWR that favored this choice are:

• Use of natural uranium as fuel, which obviates the need for developing fuel enrichment facilities.

• High neutron economy made possible by use of heavy water as moderator, which means low requirements of natural uranium both for initial core as well as for subsequent refueling. Also fissile plutonium production (required for stage 2 of the program) is high, compared to Light Water Reactors.

• Being a pressure-tube reactor, with no high pressure reactor vessel, the required fabrication technologies were within the capability of indigenous industry.

• The technology for production of heavy water, required as moderator and coolant in PHWR, was available in the country.

The Indian PHWR design has evolved through a series of improvements over the years in progressive projects. Such improvements have been driven by, among others, evolution in technology, feedback from experience in India and abroad, including lessons learnt from incidents and their precursors, evolving regulatory requirements and cost considerations. Valuable experience gained in design, manufacture, construction, operation, maintenance and safety regulation has enabled continual evolution, improvement and refinement in the PHWR concept in a progressive manner.

1.4 HEAT TRANSPORT SYSTEMS IN NUCLEAR REACTORS

1.4.1 Heat Transport System in PHWR

The heat transport system circulates pressurized coolant (D_2O) through the reactor fuel channels to remove the heat produced by fission and fission product decay heat in the uranium fuel. This heat is carried by the coolant to the steam generators.

Functional Requirements:
The major functional requirements are either safety related or process related.

They are summarized below.

Safety Related

• Must be able to contain the effects of a postulated loss of coolant accident (LOCA) within the capability of the safety systems and to provide a path for emergency coolant flow to the fuel under the same circumstances.
• Provide process measurements which would be used to trip and shut down the reactor to maintain the system pressure within design limits.
• Maintain the integrity of the reactor coolant pressure boundary in the event of a design basis earthquake.
• Provide for the removal of decay heat by natural circulation during a total loss of pumping power condition.

Process Related

• Must be able to transport the fission heat from the fuel to the steam generators.
• At all times during reactor operation the system must provide adequate cooling of the fuel and during shutdown provide a means for removing the decay heat.
• Protect the system and components from overpressure.
• Contain the D_2O inventory with the minimum possibility of either leaking or downgrading.
• Provide containment for failed fuel during normal operating conditions.

1.5 MATERIAL UNDER INVESTIGATION

STAINLESS STEEL - GRADE 304

CHEMICAL FORMULA

C <0.08%

Cr 17.5-20%

Ni 8-11%

Mn <2%

Si <1%
P <0.045%
S <0.03%

1.5.1 Background

Grade 304 is the standard "18/8" stainless; it is the most versatile and most widely used stainless steel, available in a wider range of products, forms and finishes than any other. It has excellent forming and welding characteristics. The balanced austenitic structure of Grade 304 enables it to be severely deep drawn without intermediate annealing, which has made this grade dominant in the manufacture of drawn stainless parts such as sinks, hollow-ware and saucepans. For these applications it is common to use special "304DDQ" (Deep Drawing Quality) variants. Grade 304 is readily brake or roll formed into a variety of components for applications in the industrial, architectural, and transportation fields. Grade 304 also has outstanding welding characteristics. Post-weld annealing is not required when welding thin sections.

Grade 304L, the low carbon version of 304, does not require post-weld annealing and so is extensively used in heavy gauge components (over about 6mm). Grade 304H with its higher carbon content finds application at elevated temperatures. The austenitic structure also gives these grades excellent toughness, even down to cryogenic temperatures.

1.5.2 Key Properties

These properties are specified for flat rolled product (plate, sheet and coil) in ASTM A240/A240M. Similar but not necessarily identical properties are specified for other products such as pipe and bar in their respective specifications.

1.5.2.1 Composition

Typical compositional ranges for grade 304 stainless steels are given in table 1.2

Grade		C	Mn	Si	P	S	Cr	Mo	Ni	N
	Min.	-	-	-	-	-	18.0		8.0	-
304								-		
	max.	0.08	2.0	0.75	0.045	0.030	20.0		10.5	0.10
	Min.	-	-	-	-	-	18.0		8.0	-
304L								-		
	max.	0.030	2.0	0.75	0.045	0.030	20.0		12.0	0.10
	min.	0.04	-	-		-	18.0		8.0	
304H					-0.045			-		-
	max.	0.10	2.0	0.75		0.030	20.0		10.5	

Table 1.2 Composition ranges for 304 grade stainless steel

1.5.2.2 MECHANICAL PROPERTIES

Typical mechanical properties for grade 304 stainless steels are given in table 1.3

Grade	Tensile Strength (MPa) min	Yield Strength 0.2% Proof (MPa) min	Elongation (% in 50mm) min	Hardness	
				Rockwell B (HR B) max	Brinell (HB) max
304	515	205	40	92	201
304L	485	170	40	92	201
304H	515	205	40	92	201
304H also has a requirement for a grain size of ASTM No 7 or coarser.					

Table 1.3 Mechanical properties of 304 grade stainless steel

1.5.2.3 PHYSICAL PROPERTIES

Typical physical properties for annealed grade 304 stainless steels are given in table 1.4

Grade	Density (kg/m^3)	Elastic Modulus (GPa)	Mean Coefficient of Thermal Expansion (µm/m/°C)			Thermal Conductivity (W/m.K)		Specific Heat 0-100°C (J/kg.K)	Electrical Resistivity (nΩ.m)
			0-100°C	0-315°C	0-538°C	At 100°C	At 500°C		
304/L/H	8000	193	17.2	17.8	18.4	16.2	21.5	500	720

Table 1.4 Physical properties of 304 grade stainless steel in the annealed condition

CHAPTER 2

LITERATURE REVIEW

2.1 FRACTURE

Fracture is a form of failure and is defined as separation or fragmentation of solid body into two or more parts under the action of stress, at temperature below the melting point. The process of fracture can be considered to be made up of two components crack initiation & crack propagation. Fracture can occur under all service conditions. Material subjected to alternating or cyclic loading fail due to fatigue. The fracture under such circumstances is called fatigue fracture.

Depending on the ability of material to undergo plastic deformation before the fracture two fracture modes can be defined- ductile & brittle fracture.

Figure 2.1 Illustrating fracture

2.1.1 Ductile: It is characterized by appreciable amount of plastic deformation prior to & during propagation of the crack. It is characterized by extensive plastic deformation ahead of crack tip & crack growth is stable and resists further extension unless applied stress is increased. Ductile material can absorb shock or energy (during the deformation) before failure. It occurs in most metals which are not too cold.

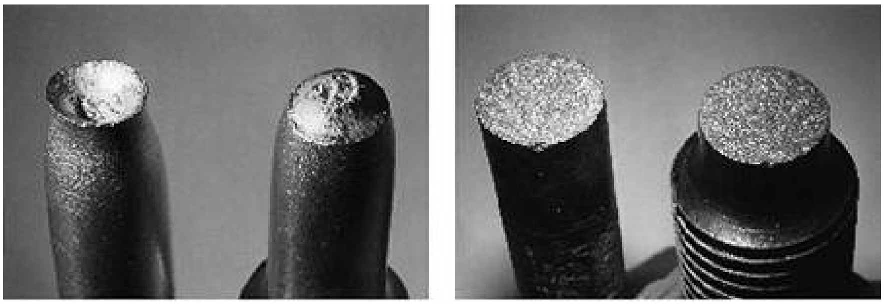

Ductile fracture Brittle fracture

Figure 2.2 Illustrating types of fracture

FCC metals are usually ductile because of the presence of large number of active slip systems.

2.1.2 Brittle: It is characterized by a rapid rate of crack propagation, with no gross plastic deformation & very little micro deformation. Crack propagates by cleavage nearly perpendicular to direction of applied stress with breaking of atomic bonds along specific crystallographic plane (cleavage plane). It is caused by decreasing temperature, increasing strain rate, triaxial stress condition. Less amount of energy absorption occurs before fracture. It occurs mostly in cold metals and ceramics. BCC & HCP metals are susceptible to brittle fracture because there are very less number of active slip planes or slip systems for plastic deformation

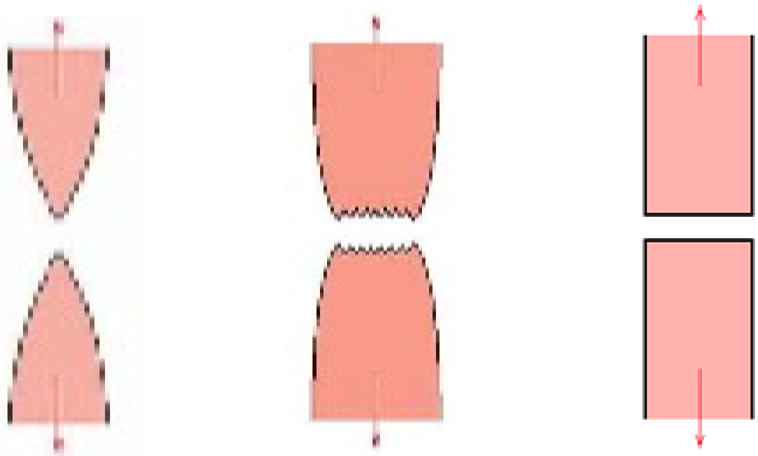

Highly ductile fracture, eg. Pure gold Moderately ductile fracture, eg. Most metal Brittle fracture

Figure 2.3 Illustrating crack propagation

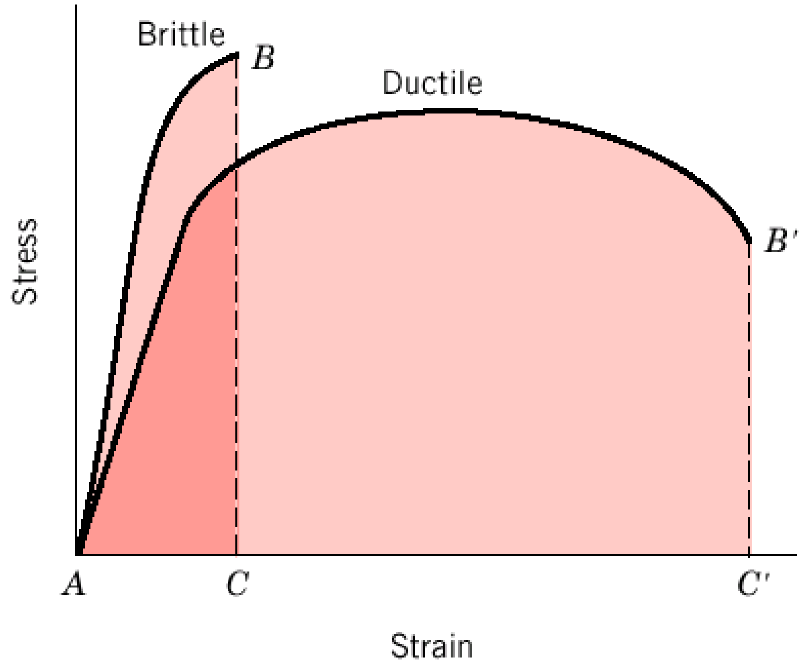

Figure 2.4 A tensile stress-strain curve

Figure above represents the degree of plastic deformation exhibited by both brittle and ductile materials before fracture.

2.2 BASICS OF DUCTILE FRACTURE

It can be divided into three categories.

2.2.1 Shear failure: It occurs as a result of extensive slip on active slip planes. It is characterized by slip on successive basal planes until the crystal separate by shear. It is observed mainly in HCP metals like Magnesium.

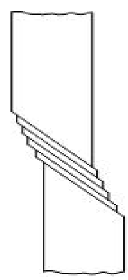

Figure 2.5 Ductile fracture by shear failure

2.2.2 Complete ductile failure: Slip occurs in many number of active slip planes in case of polycrystalline materials until it is drawn to a point before rupture. It happens in case of very ductile & pure materials like gold & lead.

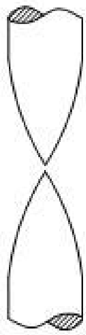

Figure 2.6 Complete Ductile Failure

2.2.3 Cup & cone type failure: Fracture begins at the centre of the specimens by the mechanism of void nucleation, growth & coalescence & then failure occurs by shear separation along the shear planes to form the cup & cone type failure.

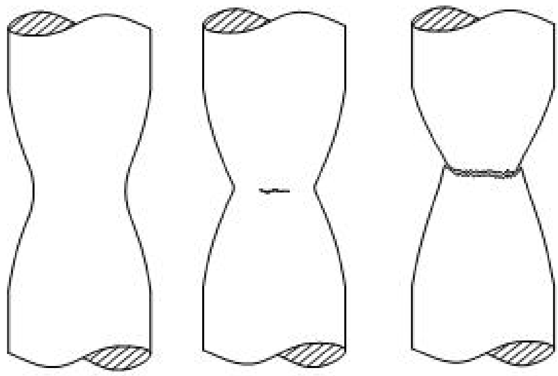

Figure 2.7 Cup & cone failure

Ductile fracture in engineering material is normally preceded by extensive plastic deformation & occurs by slow tearing of metal with considerable expenditure of energy. Ductile fracture in tension usually occurs after a localized reduction in diameter called necking & it begins to neck beyond the ultimate tensile strength, which is the maximum point in the load-elongation curve. Necking begins at the point of plastic instability where the increase in strength due to strain hardening fails to compensate for the decrease in cross sectional area, which occurs at the maximum load. The formation of necking introduces tri-axial state of stress in this region. A hydrostatic component of tension acts at the centre of the necked region. Many fine cavities form in this region & under continues straining tends to grow in size & finally coalesced. The void coalescence is synonymous with the crack formation. The crack initiates near the centre of the neck (minimum area) & propagates in a zigzag fashion, until it undergoes a large zig to the surface to form the cup & the cone of the cup-cone fracture. The ductile fracture in any engineering material involves:

- Void nucleation
- Void growth
- Void coalescence

2.3 VOID NUCLEATION

Voids, which are the basic source of ductile fracture, are nucleated heterogeneously at sites where compatibility of deformation is difficult. The preferred sites for void formation are inclusions, second phase particles or fine oxide particles in case of less purity metals. In very high purity metals, where there are no or very less number of inclusions are present, voids usually form by the mechanism of dislocation pile ups at highly distorted grain boundaries also called grain boundary triple points. Void formation can also occur by interaction among dislocations instead of interaction with grain boundary, or by interaction among twins. The mechanisms of interaction among dislocations are also known as jogs & kinks.

2.3.1 Nucleation of crack due to dislocation pile up

Dislocations usually pile up on slip planes at barriers such as grain boundaries, second phases, inclusions, or sessile dislocations, the dislocations with many branches. The leading dislocation in the pile up is acted not only by the applied shear stress, but also by the interaction force with other dislocations in the pile up. This leads to a high concentration of stress on the leading dislocation in the pile up. When many dislocations are contained in the pile up, the stress on the dislocation at the head of the pile up can approach the theoretical shear stress of the crystal. This high stress either can initiate yielding on the other side of the barrier or it can initiate a crack at the barrier.

The absence of voids on metallographic examination may not be a reliable indicator of whether void formation has occurred. It is because inclusion & second phase particles as small as 50 Angstrom have been found to nucleate voids. In the tension test, voids form prior to necking but after a neck is formed & high hydrostatic tensile stresses develop, the void formation becomes much more prominent.

Particle shapes can have an important influence on ductile fracture. When the particles are more spherical than plate like in shape as in spheroidized pearlite, cracking of the carbide is much more difficult because dislocations in the ferrite matrix can cross slip around them more easily than for plate like carbides, & thus avoid buildup of high stresses at the pile ups. The very fine rounded carbides in quenched & tempered steels are resistant to void formation & this account for the good ductility of the material **[11].** Also the second phase particles will be distorted in shape by plastic deformation processes, like rolling. So, it is common to find that the resistance to ductile fracture varies greatly with orientation in rolled sheets.

In any engineering material a number of microscopic voids are present initially in the metal matrix. These may be generated during the manufacturing process of the material or nucleate from the inclusions & second phase particles. Large particles (~1-20 μ m) are often very brittle & therefore they cannot accommodate the plastic deformation of the surrounding matrix. As a result they fail by cracking & void formation occurs. Intermediate particles (~5-500 nm) generally cannot deform as easily as the surrounding material. So when extensive plastic flow takes place in their vicinity, they lose coherence with the matrix material without any particle cracking & form voids. Particle-shape has an important influence on ductile fracture. When the particles are more spherical than plate like in shape as in spheroidized pearlite, cracking of the particle is much more difficult. In these materials the dislocations can move rather freely across spherical particles & thus avoid pile-up & build-up of high stress. So, the very fine rounded carbides in quenched tempered steels are resistant to void formation & hence ductility is more. The spacing between adjacent micro-voids is closely related to the distance between inclusions. In general, stress triaxiality promotes the void nucleation process. Thus, voids are preferably nucleated at high-constraint areas, where compatibility of deformation is minimum. In very high purity materials, where there are hardly any inclusions present, voids usually form by mechanism of dislocation pile-up at highly disordered grain boundary or other defects.

2.4 VOID GROWTH

Once voids form, further plastic strain & hydrostatic stress can cause the voids to grow. In general, voids elongates mostly in the direction of maximum principal stress. The rate of void-growth depends on other factors as the proximity of other defects, stress-field & size & shape of the void. Such void growth is more pronounced near a crack tip due to the presence of stress concentration. Most of the fracture energy associated with the micro-void coalescence is consumed during the growth of micro-voids

Growth of nucleated voids is strongly dependent on stress & strain state. Most of experiments & analyses show an exponential increase with the stress triaxiality which is defined as the ratio of the mean stress σ_m & equivalent stress $\sigma_{eq.}$

2.5 VOID COALESCENCE

As the voids grow the ligament between the voids or between the void & the crack tip start shrinking which leads to an increase in the stress level across the ligament. At some point, when the spacing among voids is of the order of their size, the stresses become unbearably high & cause an unstable necking (inter-void necking) of the ligament, which results in merging of two voids. This phenomenon is called void coalescence & is synonymous with stable crack growth. The state of stress is an important factor in determining the crack initiation & fracture strain & is generally represented by the stress triaxiality. The rate of void growth is directly related to a function of stress triaxiality & incremental plastic strain. Void coalescence leads to stable crack growth by merging of voids in the material.

All above steps are depicted in figure below.

Figure 2.8 Mechanism of ductile failure

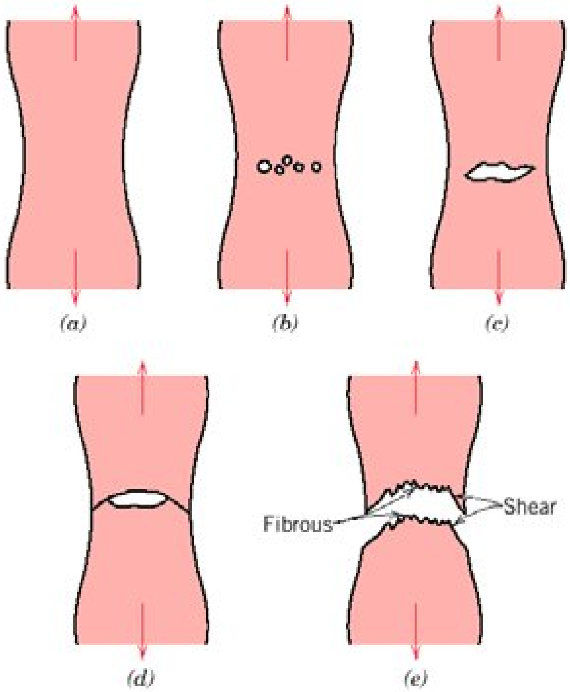

(a) Necking (b) Cavity Formation (c) Cavity coalescence to form a crack,
(d) Crack propagation (e) Fracture

2.6 MICROMECHANICAL MODELLING

These types of models aim to model ductile fracture by local approach – correlating the stress triaxiality with damage, which occurs in three stages: nucleation, growth & coalescence of voids. Constraint effects do not enter the problem as a separate issue as triaxiality of stresses enters the problem directly. Crack initiation & propagation occur with local degradation of the material losing completely its load carrying capacity. Micromechanical modelling or local approach has been extensively used in the last decade in order to analyze & predict ductile fracture behavior of different alloys. A large number of models have been developed, application of which should enable analysis of ductile fracture in a way that is to the largest extent in accordance with the natural phenomena in a material.

Application of micromechanical models should enable attunement of so-called transferability of model parameters to different geometries. Here model parameters do not mean only so called damage parameters (referring mostly to the size & number of nucleated voids in the material), but local stress & strain as well. Applications of micromechanical models should not have specific requirements related to test geometries, as the model parameters solely depend on the material. If this is really so then the advantage of such a way of analysis over the traditional process is obvious.

So far developed models for ductile fracture may be classified in two broad groups: uncoupled micromechanical models & coupled micromechanical models.

2.6.1 Uncoupled Micromechanical Models

This type of models is relatively simple & damage variable does not participate in the constitutive behaviour of the material. Here the damage & the yielding behaviour are uncoupled. The material is assumed to follow the von-Mises yield criteria with the appropriate flow & strain hardening rules (elasto-plastic properties). A damage potential symptomatic of void growth is calculated in post processing manner at large number of sampling points near the crack tip with increase in applied loads. A critical value of this parameter signifying the crack initiation in a given material is determined comparing the computed value with the experimental result for a fracture specimen. The critical value is then used to ascertain crack initiation in other real life plant components made up of same materials. This category of Modelling is called uncoupled damage Modelling. Some of these models are:

- Rice & Tracey's cavity-growth model **[1].**
- Budiansky *et al*'s model **[7].**
- Tai & Yang's model **[9].**
- Huang model.
- Chaouadi *et al'*s model.
- Dutta & Kushwaha's ψ -integral model **[16, 20].**

2.6.2 Coupled Micromechanical Models

On the past two decades, more & more attention has been paid to & research work directed towards the so-called coupled models for damage. Coupled approach to the material damage & the ductile fracture initiation considers alloy as a porous medium where the influence of nucleated voids on the stress/strain rate & plastic flow can not be avoided. In the coupled micromechanical models, one or more damage parameters are calculated to predict ductile fracture initiation. Thus, the FE analysis must include procedure for calculation for these parameters & optionally fracture initiation criterion.

These approaches have been extensively studied to different materials. In order to apply these models, there is need to find out the critical values of these parameters for the given materials. The major advantage of these models is that initiation & propagation of cracks occur naturally when the local softening due to void growth & coalescence results in the formation of a region, transmitting negligible stresses. It is not even necessary to assume an initial crack in a specimen or component, as is done in conventional fracture mechanics. Crack initiation & propagation occur when the local degradation of material has exceeded some critical value of void volume fraction over a characteristic distance. Two of the most frequently used models are:

- Rousellier Seidenfuss Model **[10, 22].**
- Gurson model **[3, 4].**

In next section, the Gurson model & its modified version Gurson Tvergaard Needleman model have been discussed in a detail which is the subject matter of this dissertation work.

2.7 GURSON TVERGAARD NEEDLEMAN MODEL [8]

Based on the work of Berg (which shows that a porous medium is governed by the normality rule), Gurson developed an approximately yield criterion & flow rule for porous ductile materials, showing the role of hydrostatic stress in plastic yield & void growth. Gurson idealized the voids as spherical or cylindrical in shape & the matrix material as rigid-perfectly-plastic material obeying von-Mises yield criterion. He calculated the stress field required for yield using a distribution of macroscopic flow fields & working through dissipation integral. The derived model originally given by Gurson is:

$$\phi(\sigma^{ij}, \sigma_m, f) = (\frac{\sigma_e}{\sigma_m})^2 + 2f \cosh\left(\frac{\sigma_k^k}{2\sigma_m}\right) - 1 - f^2 = 0,$$

Where, σ_m = tensile flow strength of the material, $\sigma_e = \sqrt{\frac{3}{2} s_{ij} \cdot s^{ij}}$, $s^{ij} = \sigma^{ij} - \sigma_k^k \cdot \overline{g}^{ij}$ represents the stress deviator, $\sigma_k^k = \overline{g}_{kj} \sigma^{kj}$, $\overline{g}_{kj} = \overline{g}_k \cdot \overline{g}_k$ is the metric tensor, σ^{kj} is the contravariant component of the macroscopic Cauchy stress tensor.

It can be noticed that for $f = 0$, the Gurson yield equation becomes von-Mises yield criterion, $\sigma_e / \sigma_m - 1 = 0$.

Or, $$\sqrt{(\sigma_1 - \sigma_2)^2 - (\sigma_2 - \sigma_3)^2 - (\sigma_3 - \sigma_1)^2 / 2} = \sigma_m$$

The original model considers that there were no interactions between voids which are not justified for modelling the final stage of void growth when coalescence of voids by localized internal necking of the matrix occurs. Tvergaard & Needleman therefore introduced an empirical modification of Gurson's yield function:

$$\phi(\sigma^{ij}, \sigma_m, f^*) = (\frac{\sigma_e}{\sigma_m})^2 + 2f^* q_1 \cosh\left(q_2 \frac{\sigma_k^k}{\sigma_m}\right) - 1 - q_3 (f^*)^2 = 0$$

The parameter q_1 was introduced by Tvergaard who analyzed the microscopic behavior of doubly periodic array of voids using a model which fully accounts for the non-uniform stress field around each void & which also accounts for the interaction between voids.

Further modifications of the plastic flow rule, made by Tvergaard & Tvergaard & Needleman, are associated with modelling the complete loss of stress carrying capacity accompanying at void coalescence occurring at void spacing of the order of void length. According to Tvergaard & Needleman, the modified void volume fraction is taken as:

$$f^*(f) = \begin{matrix} f \\ f_c + K(f - f_c) \end{matrix} \quad \text{When,} \quad \begin{matrix} f \le f_c \\ f > f_c, \end{matrix}$$

where, $K = \dfrac{f_u^* - f_c}{f_f - f_c}$; f_c is the critical value of void volume fraction at which the material stress carrying capacity starts to decay more rapidly due to void coalescence; f_f is the actual void volume fraction associated with the complete loss of stress carrying capacity. At this point f^* becomes f_u^*. The parameter K defines slope of the sudden drop of load on the load — ΔD curve & is often referred as the 'accelerating factor'.

2.8.1 Flow rule

The strain increment ($\dot{\eta}_{ij}$) in a ductile solid can be written as the sum of the elastic part ($\dot{\eta}_{ij}^{e}$) & plastic part ($\dot{\eta}_{ij}^{p}$):

$$\dot{\eta}_{ij} = \dot{\eta}_{ij}^{e} + \dot{\eta}_{ij}^{p} .$$

The elastic part ($\dot{\eta}_{ij}^{e}$) is obtained from Hook's law. Since the material satisfies the normality rule based on the von-Mises yield criterion, the macroscopic plastic strain increment satisfies

$$\dot{\eta}_{ij}^{p} = \Lambda \frac{\partial \phi}{\partial \sigma_{ij}} .$$

The scalar quantity (Λ) is determined by the strain hardening behavior of the matrix material. The equivalent plastic strain-rate in the matrix material is obtained from the plastic work expression & the work hardening properties of the matrix by the relation:

$$\sigma^{ij} \dot{\eta}_{ij}^{p} = (1 - f) \sigma_M \dot{\varepsilon}_M^{p}$$

Where, $\dot{\varepsilon}_M^{p} = \left(\dfrac{1}{E_t} - \dfrac{1}{E}\right) \dot{\sigma}_M$.

Here 'E' is the Young's modulus & 'E_t' is the current tangent modulus of the matrix material.

The uniaxial stress-strain behavior of the material is to be presented by a piecewise power-law of the form:

$$\varepsilon = \begin{cases} \dfrac{\sigma}{E} & \text{for,} \quad \sigma \le \sigma_y \\ \dfrac{\sigma_y}{E}\left(\dfrac{\sigma}{\sigma_y}\right)^n & \quad\quad\;\; \sigma > \sigma_y . \end{cases}$$

Here σ & ε are the true stress & true strain in uniaxial tension, respectively, & σ_y is the initial matrix yield strength. Accordingly, E_t is given in the terms of matrix flow strength σ_M by:

$$E_t = \frac{E}{n}\left(\frac{\sigma_M}{\sigma_y}\right)^{1-n} .$$

The increase in the void-volume-fraction, 'f' arises partly from the growth of existing voids & partly from the nucleation of the new voids, so that:

$$\dot{f} = \dot{f}_{growth} + \dot{f}_{nucleation} .$$

Since the matrix material is plastically incompressible,

$$\dot{f}_{growth} = (1-f)\bar{g}^{ij}\,\dot{\eta}^{p}_{ij} .$$

The void nucleation rate can be described by the simple two-parameter relation as suggested by Chu & Needleman

$$\dot{f}_{nucleation} = A\left(\frac{EE_t}{E-E_t}\right)\dot{\varepsilon}^{p}_{M} + \frac{1}{3}B(\sigma^k_k)$$

Where A gives the dependence of the void rate on the matrix effective plastic strain increment & B gives the dependence on the rate of increase of the hydrostatic stress.

For nucleation controlled by plastic strain the parameters are specified by:

$$A = \left(\frac{1}{E_t} - \frac{1}{E}\right)\frac{f_N}{S_N\sqrt{2\pi}}\exp\left\{-\frac{1}{2}\left(\frac{\varepsilon^p_M - \varepsilon_N}{S_N}\right)^2\right\}$$

$$B = 0$$

& for nucleation controlled by stress the parameters are specified by

$$A = B = \left(\frac{1}{E_t} - \frac{1}{E}\right)\frac{f_N}{S_N\sqrt{2\pi}}\exp\left\{-\frac{1}{2}\left(\frac{\sigma_M + \frac{1}{3}\sigma^k_k - \sigma_N}{S_N\sigma_y}\right)^2\right\}$$

Where f_N is the volume fraction of void nucleating particles, ε_N is the mean strain for nucleation & S_N is the corresponding standard deviation. Using the consistency condition $\phi = 0$,

$$\overset{\bullet}{\eta}{}^{p}_{ij} = \frac{1}{h} P_{ij} Q_{kl} \overset{\Delta}{\sigma}{}^{kl}$$

Here, $P_{ij} = \dfrac{\partial \phi}{\partial \sigma^{ij}}$

$$Q_{kl} = \frac{\partial \phi}{\partial \sigma^{ij}} + \frac{1}{3}\frac{\partial \phi}{\partial f} B \overline{g}_{ij}$$

$$h = -[(1-f) + \frac{\partial \phi}{\partial f}\overline{g}_{ij}\frac{\partial \phi}{\partial \sigma^{ij}} + \frac{EE_t (A\frac{\partial \phi}{\partial f} + \frac{\partial \phi}{\partial \sigma_M})}{(E-E_t)\sigma_M (1-f)}]\sigma^{ij}\frac{\partial \phi}{\partial \sigma^{ij}}$$

The Algorithms & mathematical expressions for finding the FE solution for this model can be found in reference. It was reported by many investigators that the prediction by the Gurson model depends on size of mesh near the crack tip. Brocks et al. Showed that even in a tensile specimen where the stress state is quite uniform, the mesh-size affects the results. Before crack formation the stress & strain fields are quite homogeneous. But as crack appears, high stress & strain gradient occur in the vicinity of crack tip & the results obtained from different mesh-size deviate from each other. The prediction of ductile fracture initiation will be therefore strongly dependant on the mesh-size at crack tip, which is rather an unpleasant effect & has hence become a popular argument against the use of damage models in fracture mechanics.

The mesh dependency may be overcome by the introduction of 'localization limiters' in the model. The basic idea is that the evaluation of the internal variables at a given material point does not only depend on the local values of state variables at this very point but also on their values in some vicinity of that point. The influence of neighboring points is limited by some weight functions decreasing with the distance. A number of proposals exist how to do this, which have proved their ability of reducing mesh sensitivity. They all require the introduction of a new material parameter – a characteristic length (l_c) or a critical volume, which determines the region of influence &

which physically, characterizes micromechanical features such as the average distance (mean free path) of inclusions

2.9 GTN MODEL PARAMETERS & THEIR DETERMINATION

Following are the GTN model parameters & their method of determination is given below briefly. The detailed procedure for determination of these parameters is explained in details in the next section of this chapter.

1. Initial void volume fraction ′f_0′: It represents the initial void fraction of the inclusions in the material which are not strongly adhered to the matrix. It is determined by metallographic examination in SEM. But analysis of notched tensile test confirms the parameter.

2. Critical length parameter ‘l_c’: It represents the mean spacing of inclusion which is responsible for void nucleation. It is determined by some standard relationships given in literature.

3. Mean strain of void nucleation: ε_n: It is determined by conducting tensile tests & subsequent metallographic examination..

4. Standard deviation of nucleation strain ‘S_N’: The process of nucleation follows statistical distribution. Chu & Needleman suggested a Gaussian distribution for the instantaneous volume fraction of nucleated voids with different values of strain. ε_N represents mean strain of this nucleation & S_N represents the standard deviation of nucleation strain. S_N is assumed generally as 0.1 for steel. It doesn’t have much effect on the results of analysis. It represents the scatter of nucleation strain. It can be determined from metallographic study of nucleation process of voids & finding the statistical distribution.

5. Void volume fraction at saturated nucleation ′f_N′: It is determined by metallographic examination as well as fitting of numerical analysis data with experimental data

6. Final void volume fraction at fracture ‘f_f’: It is determined by metallographic examination.

7. ‘q_1’ = 1.5, ‘q_2’ = 1.0, ‘q_3’ = 2.25: These values are usually not changed. But some studies suggest that these parameters are also material dependent. For this dissertation work, the values are assumed constant.

8. Critical Void volume fraction ′f_c′: It is determined by numerical fitting of the point of drop of experimental load-deflection curve of the notched tensile specimen.

2.10 REVIEW OF WORK

In 1913, a man named C.E. Inglis looked at a thin plate of glass (?) with an elliptical hole in the middle in a new and different way. Theoretically, the plate was infinitely large and the hole very small in comparison. The plate was pulled at both ends perpendicular to the ellipse.

He found that point A, at the end of the ellipse, was feeling the most pressure. He also found that as the ratio of a/b gets bigger (the ellipse gets longer and thinner) that the stress at A becomes greater and greater.

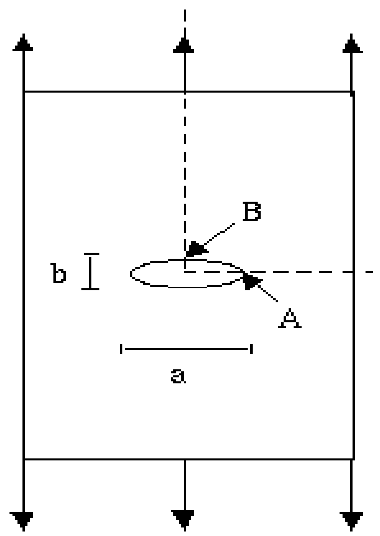

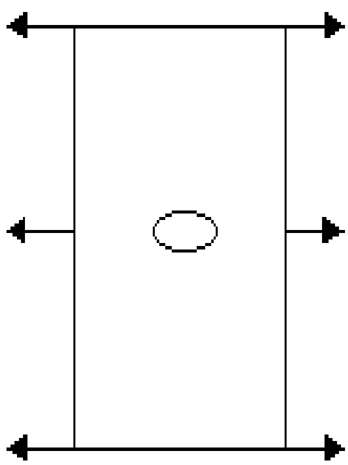

He also found that pulling on the plate in a direction parallel to the ellipse does not produce a great stress at A. This leads to the fact that a load perpendicular, not parallel, to the crack will make it grow

Then he looked at other plates with not-quite-elliptical holes, like these. From looking at these he realized that it's not really the shape of the hole that matters in cracking. What matters is the length of the crack that is perpendicular to the load and what the radius of curvature at the ends of the hole is. The longer the hole (or crack), the higher the stress, and the smaller the radius of curvature, the higher the stress. His first experiment was on a soft iron wire, 100 inches long and 0.028 inches in diameter. He pulled on this wire until it yielded. Then he took another wire with the same dimensions and put very small fractures, scratches, on it spirally. He pulled on this wire until it yielded. The scratched wire had only a quarter of the strength of the unscratched wire. He concluded that the scratches increased the stress in the wire by 3 or 4 times which made it yield earlier

He also tested a thin plate of glass, pulled in tension, with a crack in the middle perpendicular to the load. He found that the stresses at the ends of the crack were very high and the crack weaked the glass significantly.

From these two tests he concluded that materials that are fractured, no matter how small the fracture, act much differently than the same material that is without cracks!

Griffith also introduced the notion of energy sources and sinks in crack propagation which was mentioned earlier. He said that for a crack to grow, it was necessary for their to be enough potential energy in the system to create the new surface area of the crack. He did not know that it takes more than this for a crack to grow though

Then, in the 1920's, a man named A.A. Griffith extended Inglis' work. Griffith thought again about the infinite plate under tension, but he stretched the ellipse out into a crack. He did some experiments too.

A. S. argon et al [2] examined the previously proposed conditions for cavity formation from equiaxed inclusions in ductile fracture. Critical local elastic energy conditions are found to be necessary but not sufficient for cavity formation. The interfacial strength must also be reached on part of the boundary. For inclusions larger than about 100Å the energy condition is always satisfied when the interfacial strength is reached and cavities form by a critical interfacial stress condition. For smaller cavities the stored elastic energy is insufficient to open up interfacial cavities spontaneously. Approximate continuum analyses for extreme idealizations of matrix behavior furnish relatively close limits for the interfacial stress concentration for strain hardening matrices flowing around rigid non-yielding equiaxed inclusions. Such analyses give that in pure shear loading the maximum interfacial stress is very nearly equal to the equivalent flow stress in tension for the given state of plastic strain. Previously proposed models based on a local dissipation of deformation incompatibilities by the punching of dislocation loops lead to rather similar results for interfacial stress concentration when local plastic relaxation is allowed inside the loops. At very small volume fractions of second phase the inclusions do not interact for very substantial amounts of plastic strain. In this regime the interfacial stress is independent of inclusion size. At larger volume fractions of second phase, inclusions begin to interact after moderate amounts of plastic strain, and the interfacial stress concentration becomes dependent on second phase volume fraction. Some of the many reported instances of inclusion size effect in cavity formation can thus be satisfactorily explained by variations of volume fraction of second phase from point to point.

V. Tvergaard, A. Needleman [7] presents Necking and failure in a round tensile test specimen is analysed numerically, based on a set of elastic-plastic constitutive relations that account for the nucleation and growth of micro-voids. Final material failure by coalescence of voids, at a value of the void volume fraction in accord with experimental and computational results, is incorporated in this constitutive model via the dependence of the yield condition on the void volume fraction. In the analyses the material has no voids initially; but high voidage develops in the centre of the neck where the hydrostatic tension peaks, leading to the formation of a macroscopic crack as the material stress carrying capacity vanishes. The numerically computed crack is approximately plane in the central part of the neck, but closer to the free surface the crack propagates on a zig-zag path, finally forming the cone of the cup-cone fracture. The onset of macroscopic fracture is found to be associated with a sharp “knee” on the load deformation curve, as is also observed experimentally, and at this point the reduction in cross-sectional area stops.

J. Chattopadhyay et al [14] concluded that Transferability of the specimen J–R/J–T curve to the component level is an important issue in the field of fracture mechanics. Towards this goal, fracture experiments have been carried out on three point bend (TPB) specimen and through wall circumferentially cracked straight pipe of 219 and 406 mm outer diameter under four point bending load. The pipe material is SA333Gr6 and TPB specimens are machined from pipes. The image processing technique has been used to measure the crack growth and crack opening displacement in pipes. Component J–R curves have been generated from the load-deflection and load-crack growth data of pipe fracture experiments. These are compared with the TPB specimen J–R curves. Power law and second order polynomial fitting are done on the specimen and component J–R curves and J–T curves are generated. Specimen and component J–T curves are compared. Maximum moments in the pipe fracture experiments are also compared with the critical moments predicted by the 'G factor', 'Z factor' and limit approach.

J. Chattopadhyay et al [15] carried out detailed finite element analyses on conventional laboratory specimens such as Centered Cracked Panel (CCP), Three Point Bend Bar (TPBB) and Compact Tension (CT) specimens to study the characteristics of crack-tip constraint parameters, Q and h. It is observed that the loss of constraint is gradual with increasing deformation for CCP, irrespective of crack depth and shallow cracked TPBB and CT geometries. Conversely, deeply cracked TPBB and CT geometries maintain high constraint to fairly high deformation levels. This paper also addresses the nature of crack-tip constraint conditions in axi-symmetric circumferentially flawed pipe (CFP). Two loading configurations are analysed: (a) CFP under axial pull only; and (b) CFP under internal pressure with associated crack-face pressure and axial pull. It is found that the axi-symmetric CFP under internal pressure exhibits lower constraint than those under pure axial pull. The radial compressive stresses resulting from internal pressure leads to stress biaxiality, which reduces the constraint.

Brocks, bernauer et al [17] presented results of a European numerical round robin on the application of constitutive equations for ductile damage to simulate tearing of a ferritic steel are presented. The analysis of deformation and failure of a standard smooth tensile specimen is used to characterize the material and identify critical damage parameters for ductile tearing. Ductile crack growth in a (CT) specimen is then numerically simulated by applying the constitutive models of Gurson or Rousselier in order to predict a J_R-curve. Although the tensile tests were satisfactorily described, two main problems arose. The first one is that the participants' results differ considerably from each other with respect to the critical damage parameter obtained in the first task and the predicted J_R-curves in the second. The reasons were partially found in the strategies for parameter identification and the non-unique definitions for crack initiation and crack growth used in the simulations. Further reasons are expected in the individual realization of the damage model in the FE programmes or user subroutines. The second problem is a general discrepancy between the simulations and the experiment: most of the predicted J_R-curves are too flat compared with the experimental one. Manifold conclusions can be drawn for future work aiming at improving the reliability of the numerical models and promoting their application in engineering

B k dutta , H S kushwaha [18] concluded that Mesh dependency of cavity growth model due to Rice and Tracey has been overcome by integrating it over a process zone surrounding the crack tip. This integral represents a modified damage potential. The critical value of the integral for crack initiation in SA333Gr.6 material has been determined analysing a CT specimen and comparing the computed J with the experimentally measured J-initiation value. The critical value of the integral was then used to compute J-initiation in other fracture specimens having different crack-tip constraints. The critical value was also used to predict crack initiation loads in three 8 in. straight pipes and three 8 in. elbows having different measure of through-wall circumferential flaws. The computed values have been compared with the experimentally measured values. A close agreement between the computed crack initiation loads with the experimentally measured values justified the usefulness of the present modified damage potential.

B.K. Dutta, et al [19] describes that the the structural integrity of components is usually performed using the specimen fracture resistance curve. However, the specimen fracture resistance curve significantly differs from the component fracture resistance. This is the most serious limitation of classical fracture mechanics. To address this issue, several tests have been carried out on fractured specimens and piping components under an Indo-German bilateral project. Two approaches, namely, two-parameter fracture mechanics and micro-mechanical models are considered to investigate the feasibility of transferability. For the two-parameter fracture mechanics approach, the J-integral has been used as the crack driving force and q is used as a measure of stress triaxiality. The triaxiality quotient q is proportional to the ratio of the hydrostatic stress and the von

Mises effective stress and is an additional parameter to make a decision about the initiation value of the J-integral for the failure behaviour of a component. It is shown that if the triaxial conditions match for any two arbitrary geometries, it is feasible to transfer the fracture parameters. The difficulty in transferability is largely overcome by damage mechanics, which models the drop in load carrying capacity of a material with increase in plastic strain. Such modeling is done considering nucleation, growth and coalescence of voids in a material following large-scale plasticity. The Gurson–Tvergaard–Needleman and Rousselier models are used. Some of the results obtained by these models and comparisons with experimental results are presented in this paper to demonstrate the usefulness of damage mechanics in analyzing components with flaws.

S. Acharyya, et al [21] described that the micro mechanical model by Gurson–Tvergaard–Needleman is widely used for the prediction of ductile fracture. Some material properties (Gurson parameters) used as material input in this model for simulation are estimated experimentally from specimen level. In this article an attempt has been made to tune the values of some of these Gurson's parameters by comparing the simulated results with the experimental results in the specimen level (axisymmetric tensile bar and CT specimens). An elastic–plastic finite element code has been developed together with Gurson–Tvergaard–Needleman model for void nucleation and growth. The initial value of f c is determined from Thomason's limit load model and then tuned on the basis of best prediction of the failure of one-dimensional tensile bar. Then the load versus load line displacement and J versus Δa results for CT specimen are generated with the same code and the value of f n is tuned to match the simulated J versus Δa results with the experimental results. Lastly the same code and the Gurson's parameters obtained are used to simulate the load versus load point displacement and crack growth for pipe with circumferential crack under four point bending. The simulated results are compared with the experimental results to assess the applicability of the whole method. In the proposed material modelling, post-yielding phenomena and necking of the tensile bar are simulated accordingly and strain softening due to void nucleation and growth has been taken care of properly and drop in stress is implicitly simulated through a model. Incremental plasticity theory with arc length method is used for the nonlinear displacement control problem.

CHAPTER 3

PROBLEM DEFINITION

3.1 AIM OF THE THESIS

The primary heat transport (PHT) piping of any nuclear reactor is a critical system. This PHT piping of pressurized heavy water reactor (PHWR) mainly consists of five pipelines. These are steam generator inlet, steam generator outlet, pump discharge line, reactor inlet header and reactor outlet header respectively. Heavy water comes out of the reactor and enters reactor outlet header via the feeder lines. Coolant from the reactor outlet header enters steam generator inlet and then enters main primary pump through steam generator outlet. From the pump, coolant enters the reactor inlet header via pump discharge line and from reactor inlet header coolant enters the reactor core through the feeder lines. Figure 3.1 shows a typical layout of the flow path in a typical PHWR. Any failure of this system will lead to very grace consequences, not speaking of huge monetary losses resulting from non utilization of the reactor setup. Hence, it is necessary to have an accurate and reliable method of predicting the fracture behviour in such components.

Fracture resistance of a ductile material is conventionally characterized by J-Resistance curves obtained from different fracture specimens. The original idea was that a unique fracture resistance curve would suffice to characterize the material .However testing of different specimens revealed considerable J_R curves **[12].** The standards for fracture testing often enforce high constraint conditions in specimen to obtain a conservative index of material toughness. The application of J_R curves from these specimens to low constraint structural application introduces high degree of conservatism. The total conservatism inherent in a particular design can become excessively large and the true safety factor is not known. A reverse problem occurs when the fracture toughness data are obtained on relatively low constraint specimens and then used in high constraint applications. This would make the design non-conservative. Thus the conventional fracture mechanics based on single parameter criteria is not adequate to model the fracture process **[13].**

Under such circumstances it is advisable to use damage mechanics (micro mechanical analysis) the difficulty of geometry independency is largely overcome by the damage mechanics, which model the drop in load carrying capacity of a material with the increase in plastic strain such modeling is done considering nucleation, growth and coalescence of the voids in a material following large scale plasticity. There are a wide variety of techniques available in damage mechanics of them, gurson modal [3] is one of the most powerful models and used successfully by researchers throughout the world. This constitutive model introduced by gurson and modified by tvergaard and Needleman has been used in this work to predict ductile fracture.

So, the aim of present work is to determine gurson parameter from analysis of different specimen and assess the fracture characteristics of SS 304 reactor grade steel using CT geometry.

CHAPTER: 4

EXPERIMENTATION

4.1 INTRODUCTION

Gurson Material parameters are determined by curve fitting of experimental and analytical results. The curve fitting is generally done using load-ΔD curves of round notched tensile specimens. In curve fitting process the Gurson parameters are varied so that the analytical curve approximates the experimental one in terms of load dropping point and slope of curve at sudden load drop. The experiments were performed at BARC and IIT Roorkee and data was provided. This chapter describes the results of tests conducted for damage mechanics analysis.

4.2 MATERIAL PROPERTIES

The material studied is SS 304 reactor grade steel. The mechanical properties of material are given in Table 4.1

Material Properties	**Value**
Young's Modulus	.193 x 10^6 GPa
Ultimate Tensile Strength	515 Mpa
Yield strength	205 Mpa
Poisson's Ratio	0.29
% Elongation	40%

Table: 4.1 Mechanical properties of SS 304 at room temperature

Stress strain curves for SS304 are shown in Figure 4.1 and 4.2.

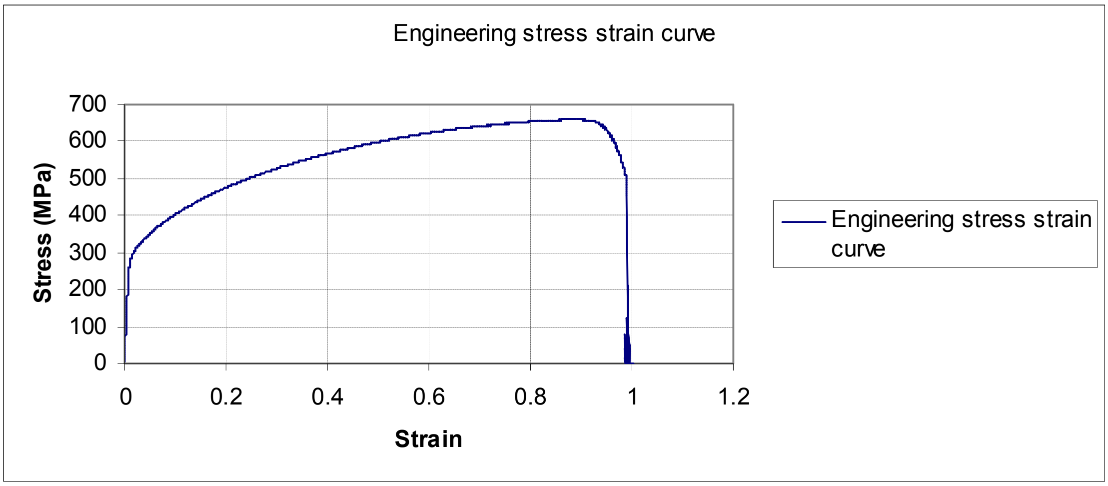

Fig 4.1 Engineering stress-strain curve of SS304

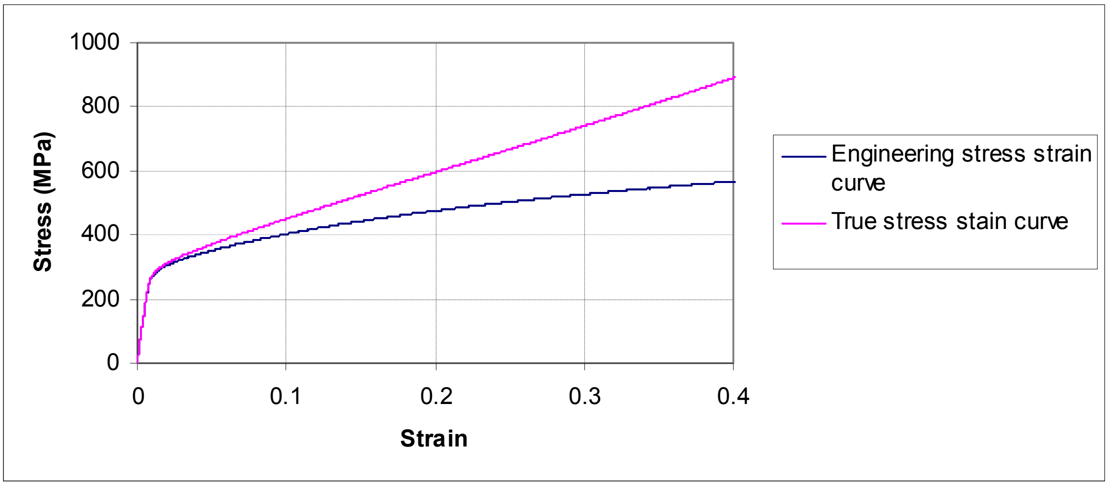

Fig 4.2 Engineering stress-strain vs. True stress strain curve of SS 304

4.3 EXPERIMENTAL LOAD – DIAMETRIC CONTRACTION CURVES OF ROUND NOTCHED TENSILE SPECIMENS

Tensile test results of RNTS were taken from RSD, BARC. Results were given in the form of time vs. load and material diametric contraction was recorded using digital camera which takes 25 images per second. These images were processed to find diametric contraction of round notch tensile specimen.

4.3.1 Details of the Round Notched Tensile Specimens

There were two notched tensile specimens with notch groove radius 2mm and 4mm, designated as RNTS R2 and RNTS R4. The geometry of specimens is shown in Figure 4.3.

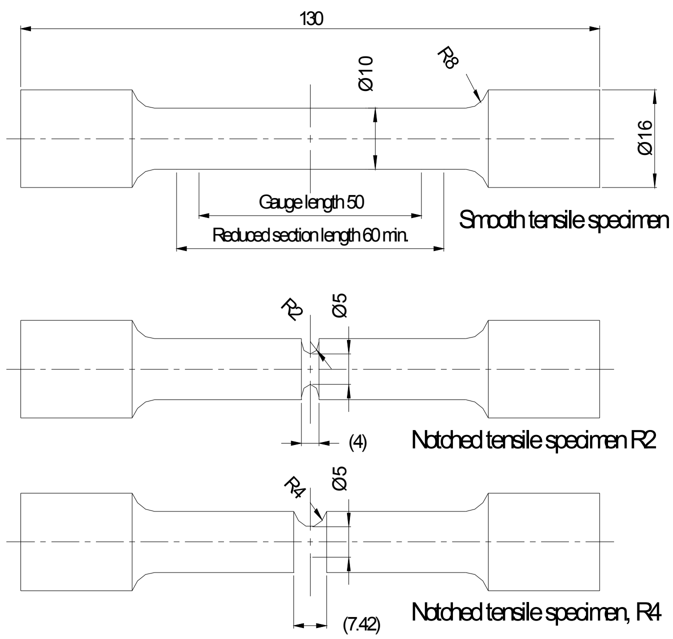

Figure 4.3 Detail of smooth and notched tensile specimens

The results of tests were recorded in the form of images (Figure4.4) and instantaneous load values from the digital display. The images were then post-processed with AutoCAD software (Figure 4.5). The images were copied and pasted in Photoshop. Then the round piece diameter and notch diameter were measured. The notch diameter was calculated by taking the reference diameter of cylindrical part as 10mm.

Let measured notch diameter =d

Cylindrical part diameter =D

Now as we know that the diameter of cylindrical part is 10mm

So we can find out notch diameter as:

Notch diameter = (d/D) x 10 mm

Diametric contraction (ΔD) = Initial Notch diameter –Notch diameter

Initial notch diameter was 5mm.

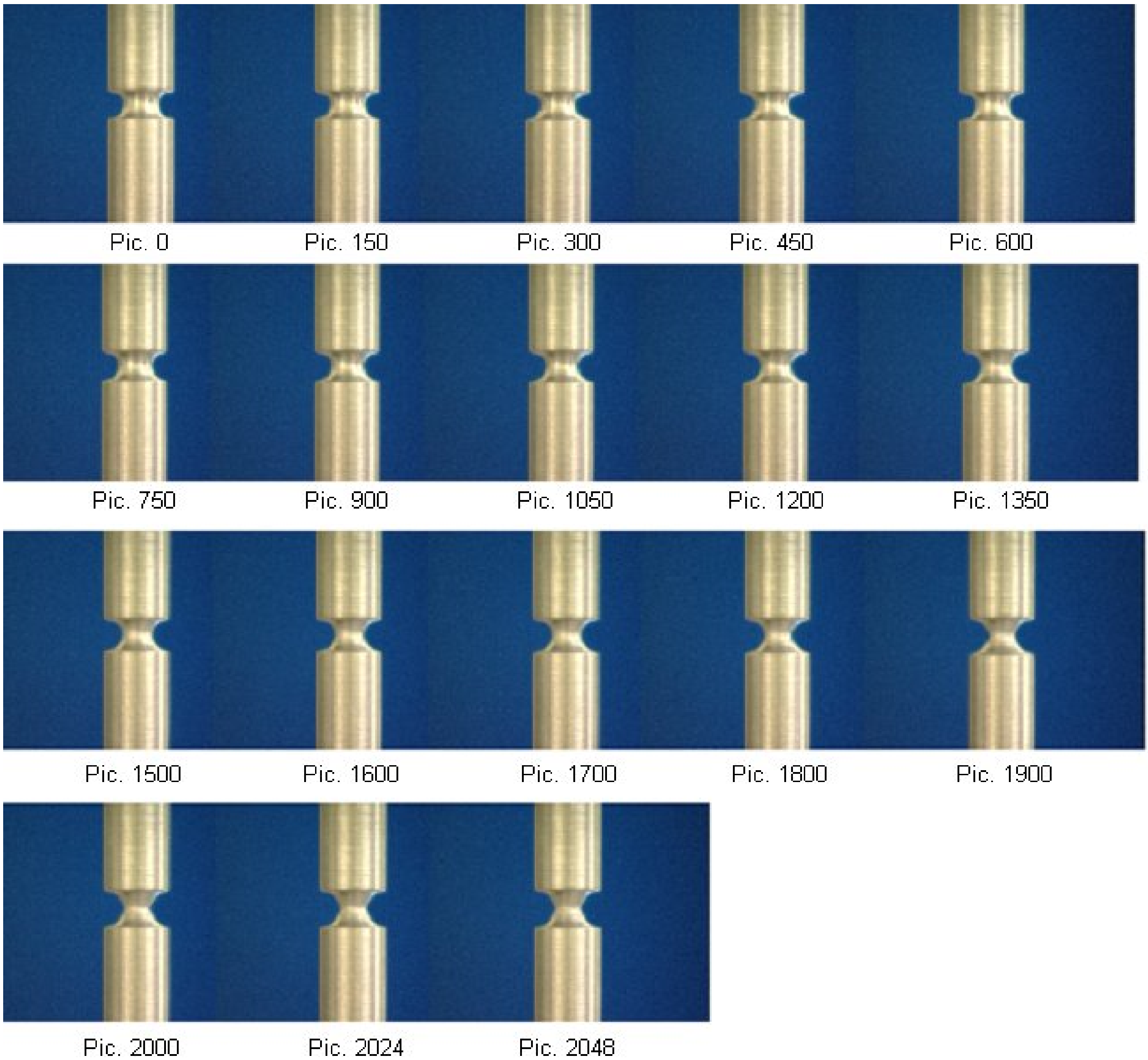

Figure 4.4 Photographs during testing (SS304 R2)

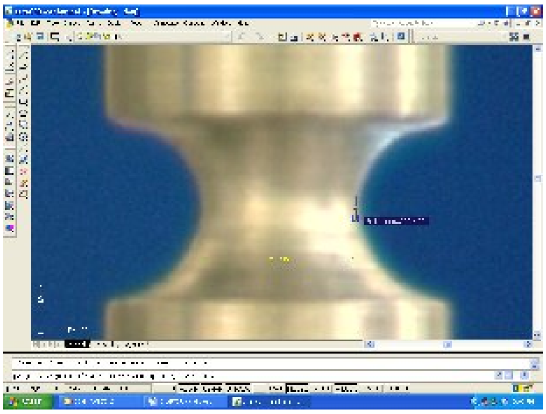

Figure 4.5 The image processing using AutoCAD

4.3.2 Test results

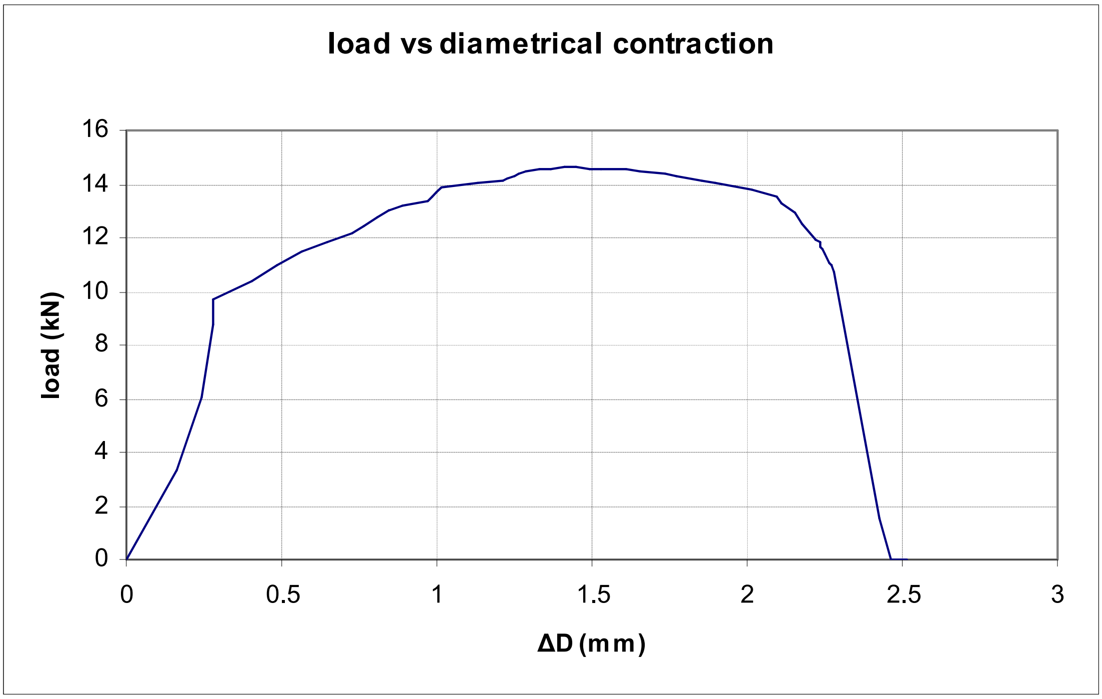

Figure 4.6 Experimental Load-ΔD curve for R2

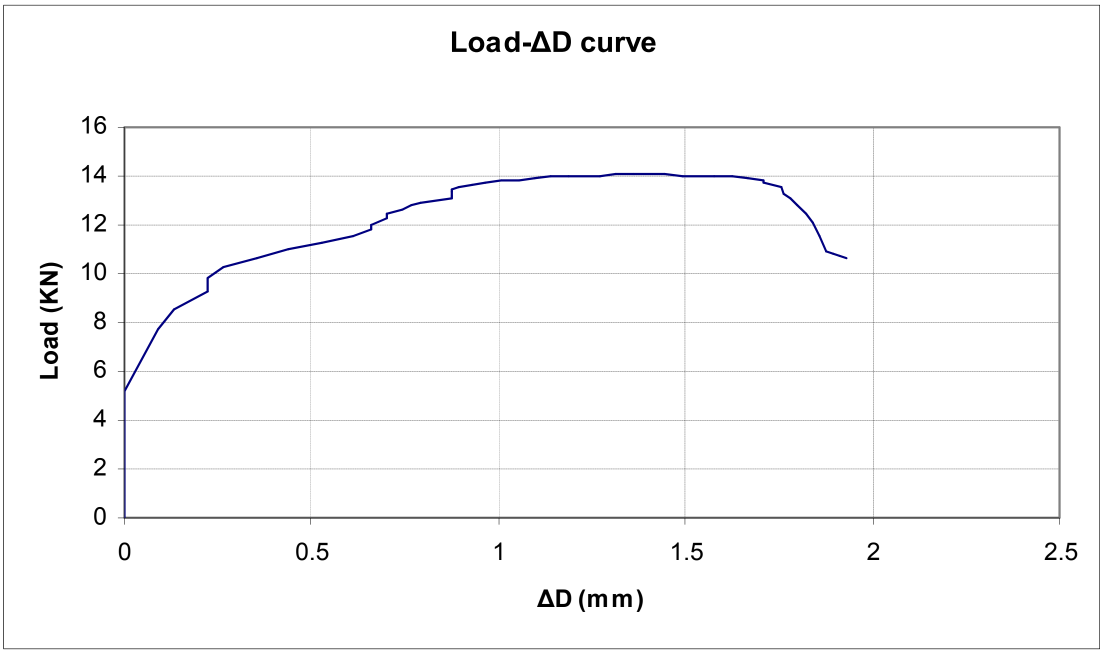

Figure 4.7 Experimental Load-ΔD curve for R4

CHAPTER 5

ANALYSIS METHODOLOGY

The FE analysis adapted for this work can be divided into 5-steps:

i. Generation of input file for creating the FEM shape of the specimen
ii. Running the above input file for creating the mesh
iii. Making the input file for analysis
iv. Running the FE code **MADAM** (**M**aterial **D**amage **M**odeling)
v. Post-processing the output from FE code

5.1 GENERATION OF INPUT FILE FOR CREATING THE SHAPE OF THE SPECIMEN

5.1.1 The Round Notched Tensile Specimen

The mesh for the notched tensile specimen were generated by an in house generated FORTRAN code **FEMSHAPE** which requires an input file which contains the details regarding the specimen. As the specimen has two axis of symmetry, only one fourth of the specimen was modeled. The geometric model was made in such a way that the mesh size near the crack propagation direction was equal to two times the critical length parameter l_c (mesh size = $2l_c$).meshes away from the crack path were intentionally made larger to reduce the computational time. The input file is written in the following format:

1^{st} Line

First data: Number of Global Elements.
Second data: Number of Global Nodes.

2^{nd} Line

First data: Name of The Element.
Second data to ninth data: Name of the node in clockwise direction writing first the corner nodes and then the middle nodes.
Tenth data: Number of division in X direction.
Eleventh data: Number of division in Y direction.

$3rd$ Line to Last Line

Contains weight age of total number of (X+Y) divisions with eight values in one row. Giving the weight age of X divisions first.
Repeat the second line to last line for all the elements

In the last write X and Y coordinates of all the global nodes.

Example illustrating the above format:

```
  8   39
   1    1    2    3    4    5    6    7    8   12    3
   1.0000   1.0000   1.0000   1.0000   1.0000   1.0000   1.0000   1.0000
   1.0000   1.0000   1.0000   1.0000
   1.0000   1.0000   1.0000
   2    4    3    9   10    7   11   12   13   12    3
   1.0000   1.0000   1.0000   1.0000   1.0000   1.0000   1.0000   1.0000
   1.0000   1.0000   1.0000   1.0000
   1.0000   1.0000   1.0000
   3   10    9   14   15   12   16   17   18   12    3
   1.0000   1.0000   1.0000   1.0000   1.0000   1.0000   1.0000   1.0000
   1.0000   1.0000   1.0000   1.0000
   1.0000   1.0000   1.0000
   4   15   14   19   20   17   21   22   23   12    3
   1.0000   1.0000   1.0000   1.0000   1.0000   1.0000   1.0000   1.0000
   1.0000   1.0000   1.0000   1.0000
   1.0000   1.0000   1.0000
   5   20   19   24   25   22   26   27   28   12    3
   1.0000   1.0000   1.0000   1.0000   1.0000   1.0000   1.0000   1.0000
   1.0000   1.0000   1.0000   1.0000
   1.0000   1.0000   1.0000
   6   10   15   31   32   18   37   33   36    3   10
   1.0000   1.0000   1.0000
   1.0000   1.5000   2.0000   2.5000   3.0000   3.5000   4.0000   4.5000
   5.0000   5.0000
   7   15   20   30   31   23   38   34   37    3   10
   1.0000   1.0000   1.0000
   1.0000   1.5000   2.0000   2.5000   3.0000   3.5000   4.0000   4.5000
   5.0000   5.0000
   8   20   25   29   30   28   39   35   38    3   10
   1.0000   1.0000   1.0000
   1.0000   1.5000   2.0000   2.5000   3.0000   3.5000   4.0000   4.5000
   5.0000   5.0000
1        0.000000       0.000000
2        2.500000       0.000000
3        2.652240935    0.765366865
4        0.0000000      1.863961031
5        1.250000       0.000000
```

6	2.538429439	0.390180644
7	1.326120467	1.314663948
8	0.000000	0.931980515
9	3.085786438	1.414213562
10	0.000000	4.5000000
11	2.837060775	1.111140466
12	1.542893219	2.957106781
13	0.000000	3.181980515
14	3.734633135	1.847759065
15	2.636038969	4.500000
16	3.388859534	1.662939225
17	3.185336052	3.173879533
18	1.493196129	4.500000
19	4.500000	2.000000
20	4.500000	4.500000
21	4.109819356	1.961570561
22	4.500000	3.2500000
23	3.604894347	4.5000000
24	5.000000	2.000000
25	5.0000000	4.500000
26	4.750000	2.000000
27	5.000000	3.2500000
28	4.750000	4.500000
29	5.000000	30.000000
30	4.5000000	30.00000
31	2.636038969	30.00000
32	0.000000	30.000000
33	1.493196129	30.000000
34	3.604894347	30.00000
35	4.750000	30.000000
36	0.000000	17.25
37	2.636038969	17.25
38	4.500000	17.25
39	5.0000000	17.25

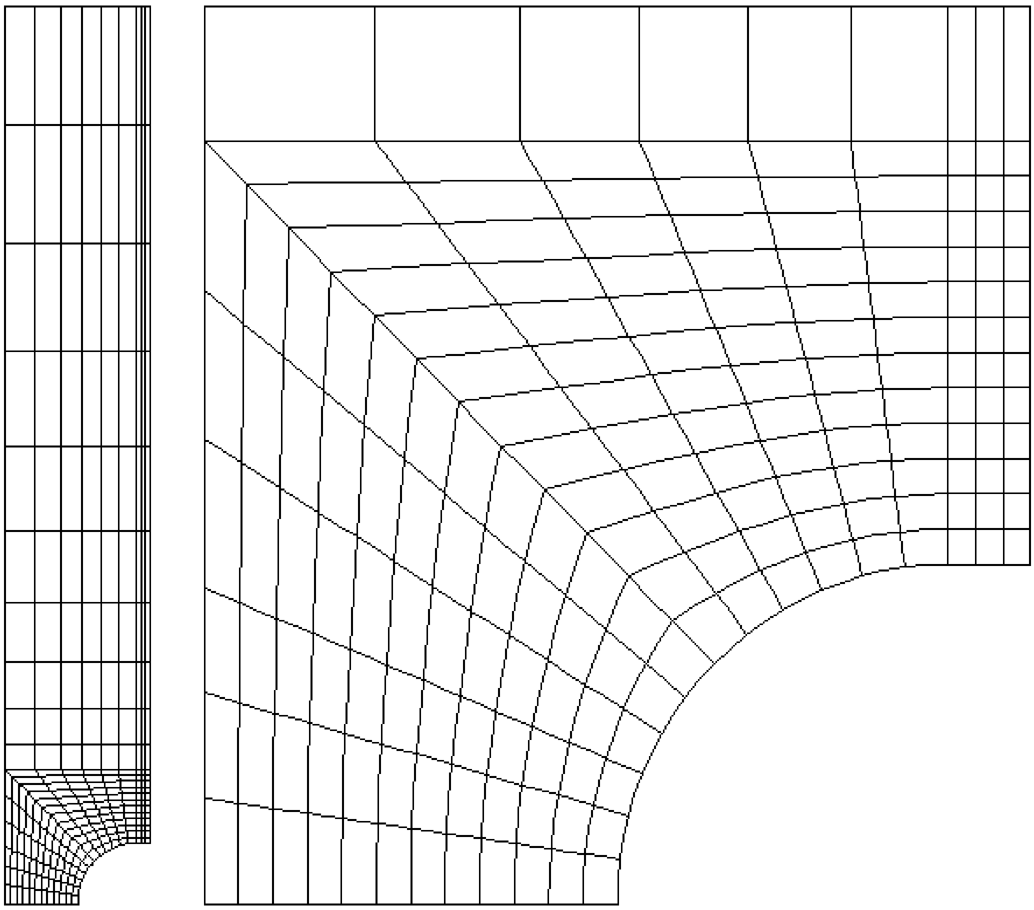

Figure 5.1 FE mesh for RNTS R2 specimen

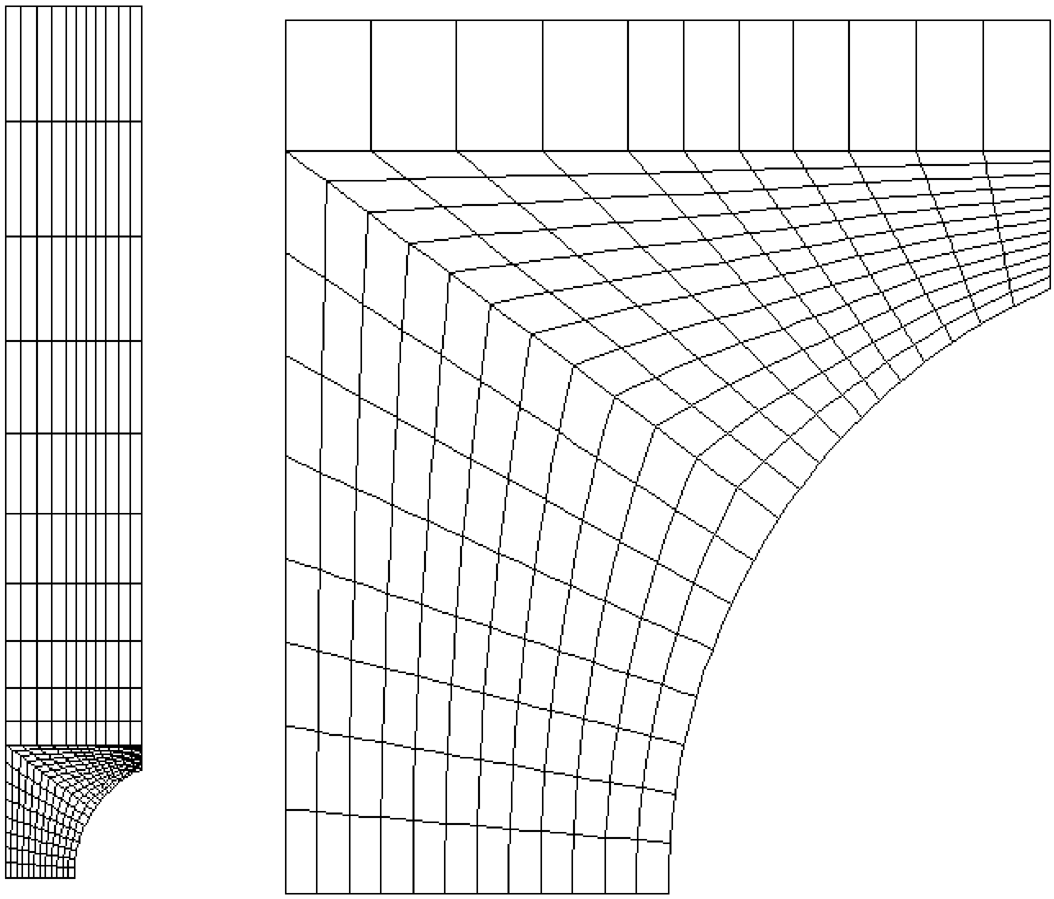

Figure 5.2 FE mesh for RNTS R4 specimen

5.1.2 Compact tensile specimen (CT)

For the CT specimen, as there was a single axis of symmetry along the crack plane so only half of the specimen was modeled. Mesh was generated by an in house generated FORTRAN code **FEM-CT** which requires an input file which contains the details regarding the specimen. The input file is written in the following format:

1^{st} **Line**

First data: - Starting node number
Second data: - Starting element number
Third data: - Number of X Divisions at the base
Fourth data: - Number of fine layers
Fifth data: - X coordinate of Bottom Left Corner
Sixth data: - Y coordinates of Bottom Left Corner

$2^{nd}-10^{th}$ **Line**

Contains weight age of all X Divisions with Eight values in one row

11^{th} **Line**

Y dimension of Fine layered Elements

12^{th} **Line**

Number of transitions

13^{th} **Line**

First data: - value of Y1
Second data: - value of Y2

14^{th} **Line**

Number of division in Y3

15^{th} **Line**

Contains weight age of Divisions in Y3
Example illustrating the above format:

```
1    1  72    4      0.000     0.000
3.80 3.60 3.00 2.80 2.60 2.40 2.20 2.00
1.80 1.60 0.50 0.40 0.40 0.30 0.30 0.30
0.30 0.30 0.30 0.30 0.20 0.20 0.20 0.20
```

0.20 0.20 0.20 0.20 0.20 0.20 0.20 0.20
0.20 0.20 0.20 0.20 0.20 0.20 0.20 0.20
0.20 0.20 0.20 0.20 0.20 0.20 0.20 0.20
0.20 0.20 0.20 0.20 0.20 0.20 0.20 0.20
0.20 0.20 0.20 0.20 0.80 1.30 1.50 1.70
2.00 2.00 2.00 2.00 2.00 2.00 2.00 3.50
0.2 0.2 0.2 0.2
2
0.5 1.2
5
2.5 5.0 8.0 9.5 12.5

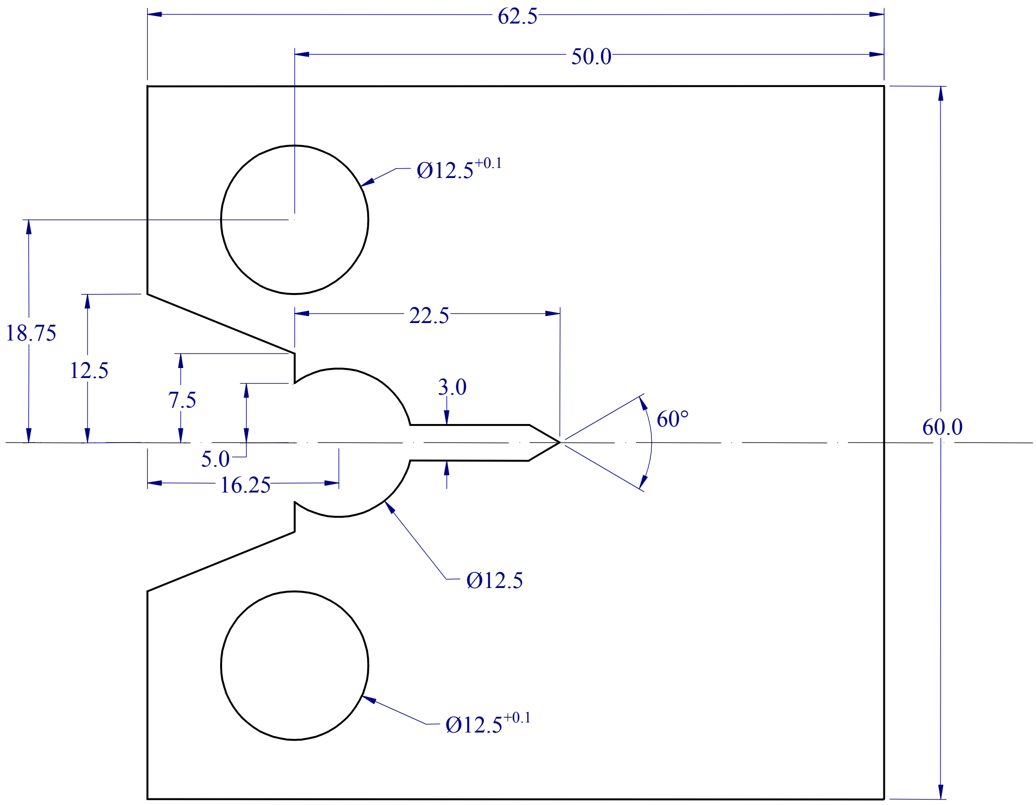

Fig 5.3 CT Specimen being used for fracture testing with Dimensions according to ASTM E-1820 standard

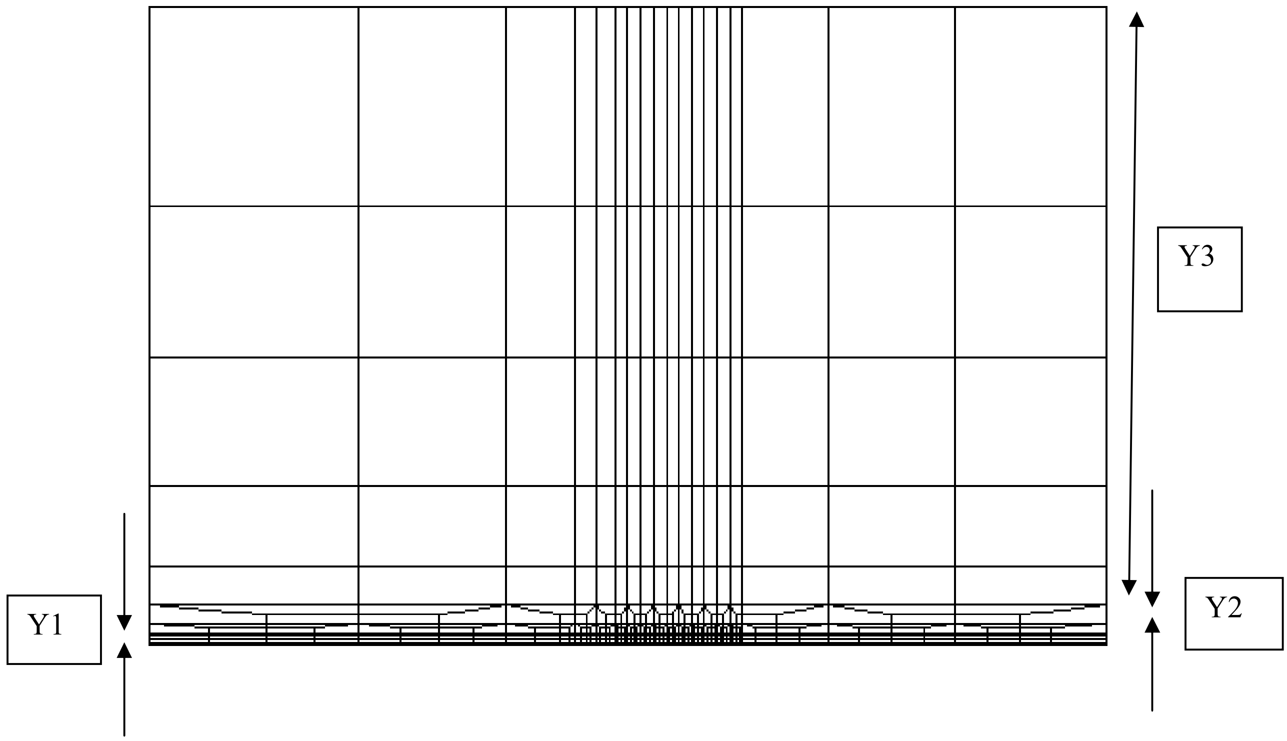

Figure 5.4 PLOT OF MESH OF CT SPECIMEN

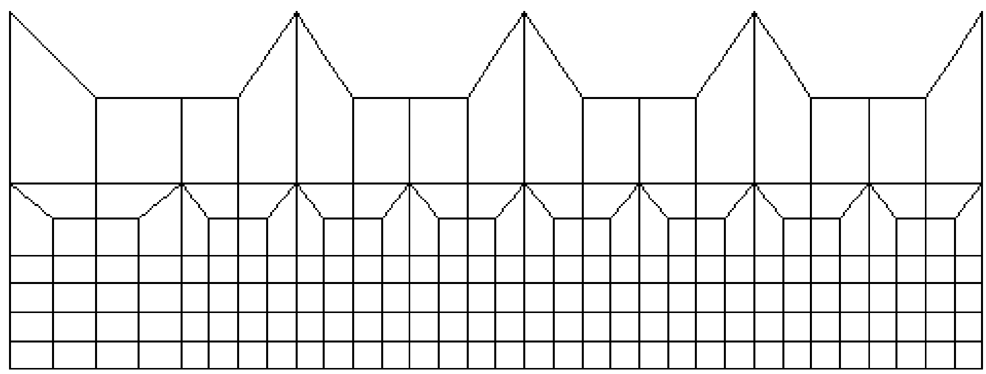

5.2 MAKING THE INPUT FILE FOR ANALYSIS

Once the mesh had been constructed the next step was to prepare the input file for the component giving every detail that describes actual problem under investigation. The input file was then used by MADAM code. The input file was written in the following format:

Card-set 1

First word (a10): Name of equation solver- SPARSE, FRONTAL, COLSOL (Column solver), LPCG (linear pre-conditioned conjugate gradient solver).

Second word (a10): solution technique- NEWTON (Newton-Raphson method), RIKS (Modified Rik's method).

Third word (a10): Integration scheme employed- MIDPOINT, BEULER (Backward Euler), FEULAR (Forward Euler).

Card-set 2

Third card set (a80) describes title to the problem.

Card-set 3

First data (i5): Total number of elements.
Second data (i5): Total number of nodes.
Third data (i5): Total number of nodes per element.
Fourth data (i5): Number of elements for which the node relations are to be provided.
Fifth data (i5): Number of nodes for which the coordinates are to be provided.
Sixth data (i5): Index for loading condition- 1 (plane stress), 2 (plain strain), 3 (axi-symmetric case), 4 (3-D case).

Card-set 4

First data (i5): Number of materials of which the specimen is made up of.
Second data (i5): type of stress strain curve- 1 (true stress true strain), 2 (engineering stress engineering strain)
Third data (i5): Type of analysis- 0 (elastio-plastic), 1 (damage mechanics).
Fourth data (i5): Index for material hardening- 0 (isotropic hardening), 1 (kinematic hardening)

Card-set 5

First data (i5): number of group of boundary conditions.
Second data (i5): Total number of boundary nodes.
Third data (i5): number of group of loads.

Card-set 6

First data (i5): Index for geometric non-linearity- 1(on), 0(off).
Second data (i5): number of load increments.
Third data (i5): Maximum number of iteration for convergence.
Fourth data (i5): Number of group of load fractions.
Fifth data (i5): Number of print interval for output files.

Card-set 7

Here element node relationship is provided which has been obtained through the mesh generating code.

For 2D 4-noded iso-parametric quadrilateral element

First data (i5): Element ID.
Second data (i5): Material ID.
Third to Sixth data (4i5): ID of corner nodes.

For 2D 8-noded iso-parametric quadrilateral element

First data (i5): Element ID.
Second data (i5): Material ID.
Third to Sixth data (4i5): ID of corner nodes. (Anticlockwise)
Seventh to tenth data (4i5): ID of corresponding mid nodes. (Anticlockwise)

For 3D 20-noded iso-parametric quadrilateral element

First data (i5): Element ID.
Second data (i5): Material ID.
Third to tenth data (8i5): ID of corner nodes. (Anticlockwise)
Eleventh to eighteenth data (8i5): ID of corresponding mid nodes. (Anticlockwise)

Card-set 8

Here the coordinate in x, y and z direction for each node are provided as obtained from mesh generating codes.

For 2D

First, fourth and eleventh data (i5): node IDs
Second, third, fifth, sixth, seventh and eighth data (2i5): x and y coordinates.

For 3D

First, fifth data (i5): node IDs

Second, third, fourth, sixth, seventh and eighth data (3i5): x, y and z-coordinates.

Card-set 9

This card contains the boundary conditions.

For 2D

First data (i5): the number of boundary nodes on the group of boundary condition.
Second and third data (3x, 2il): index for boundary condition along x and y direction (1-free BC, 0-prescribed BC).
Fourth and fifth data (2f10.3): values of displacement along x and y direction.
Sixth data (f10.3): angle of orientation of boundary node line with respect to x-axis
Seventh data (i5): number of load curves.
Next line data (16i5): the IDs of boundary nodes.

For 3D

First data (i5): the number of boundary nodes on the group of boundary condition.
Second and third data (3x, 3il): index for boundary condition along x, y and z direction (1-free BC, 0-prescribed BC).
Fourth and fifth data (2f10.3): values of displacement along x, y and direction.
Sixth data (f10.3): angle of orientation of boundary node line with respect to x-axis
Seventh data (i5): number of load curves.
Next line data (16i5): the IDs of boundary nodes.

Card-set 10

This card set contains the properties of the different materials under investigation.
First data (e10.3): young's modulus of elasticity (MPa).
Second data (e10.3): Poisson's ratio.
Third data (e10.3): yield stress (MPa).
Fourth data (i5): number of data-points provided for stress-strain curve.
Next lines (6e10.3): 3 sets of strain and stress values.

The true stress strain curves were calculated from the engineering stress strain shown as in fig . The following relations were used for computing true stress and logarithmic strain.

$$\sigma = \sigma_e \ (1+e)$$
$$\varepsilon = \ln (1+e)$$

[redacted]

Card-set 11

First to tenth data (10f9.3): this card contains the gurson parameters-

Card-set 12

First data (i5): Number of Load increments
Second Data (e10.3): Load step

Card-set 13

First line (i5): Number of damageable elements.
Second line onwards (16i5): ID of damageable elements.

Card-set 14

Here we provide nodes where the displacements and reaction are desired.

5.3 RUNNING THE FE CODE MADAM (MATERIAL DAMAGE MODELLING)

Input file was run using BARC in-house finite element code MADAM (Material Damage Modelling). MADAM has been developed based on the principles of continuum damage mechanics (Modified Gurson's model).

5.4 POST-PROCESSING THE OUTPUT FROM MADAM CODE

1. Output file: Gives the damage elements corresponding iteration number and gauss point and also confirms the input data.
2. MADAM-POST.OUT: Stores in detail the deformation history and different stress and strain values.
3. MADAM.DAT: Gives the displacement of each node and reaction of boundary nodes at specified interval.

5.4.1 Post-processing for load-ΔD and load-displacement

For RNTS, CT and TPB specimens the load-displacement values were given in MADAM.DAT file. A program was used to find the load-displacement for all specimens and also load-ΔD value for RNTS specimen.

5.4.2 Post-processing for J-R curve

For calculating J-R values jcg code was used. There were two input files to the code. First *jcg.INP file and second jcg.EXT file. In *jcg.INP file there were data regarding total number of iterations and displacement and load corresponding to each iteration and also data regarding the damage element corresponding gauss point and iteration number. Jcg.EXT file contains data regarding specimen geometry and material properties. From out put file *jcg.DAT we get J-R values and J_i (initiation) value.

CHAPTER 6

DETERMINATION OF GURSON PARAMETERS

6.1 A STUDY ON EFFECT OF GURSON PARAMETERS ON MATERIAL BEHAVIOUR

The effect of Gurson parameters on load-ΔD & J-R curve is studied by varying one parameter at a time and keeping other parameters unchanged. In the study, four criteria were considered extensively:

i. The dropping point in the RNTS load- ΔD curves
ii. The slope of sudden drop in the RNTS load- ΔD curves
iii. J_I (J-integral at crack initiation).

Gurson parameters used in study are given in Table 6.1 and same parameters were used as initial parameters.

Gurson parameters	Value
Initial void volume fraction, ‘f_o’	0.000001
Critical void volume fraction, ‘f_c’	0.05
Final void volume fraction, ‘f_f’	0.1707
Void volume fraction at saturated nucleation, ‘f_N’	0.005
Mean value of strain for nucleation, ‘ε_N’	0.3055
Standard deviation of strain for nucleation, ‘S_N’	0.1
Modifying parameters ‘q_1’ ‘q_2’ ‘q_3’	1.5 1.0 2.25
Critical length parameters ‘l_c’	0.2
Modified ultimate void volume fraction ‘f_u’	0.566

Table 6.1 Initial Gurson parameters and their values

6.2 EFFECT OF INITIAL VOID VOLUME FRACTION (F_0)

Initial void volume fraction is determined by metallographic examination and calibrated by analysis of notched tensile test specimens .It represents the initial void fraction of the inclusions in the material which are not strongly adhered to the matrix. The primary void portion of f_0, grows under increasing stress and strain of the material, while the inclusion part of the initial void volume fraction increases the probability of void nucleation. Figure 6.1 clearly shows the effect of initial void volume fraction on load dropping point for notched tensile specimens. With increase in values of f_0 there is increase in slope of load- ΔD curve.

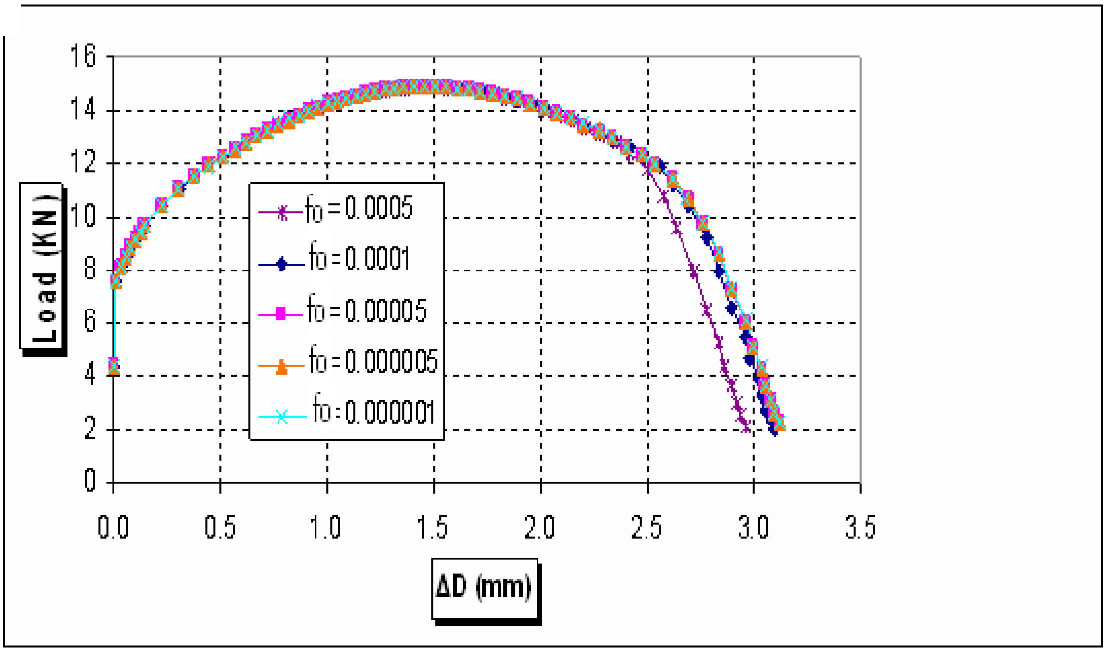

Figure 6.1 Load-ΔD curves for different f_o values

The effect of f_0 is more prominent in J-R curve as shown in Figure 6.2. The study reveals that the J-initiation is not much affected by initial void volume fraction. Table 6.2 gives the ΔD (at sudden load drop), Slope Load-ΔD and (initiation) for different values of FO

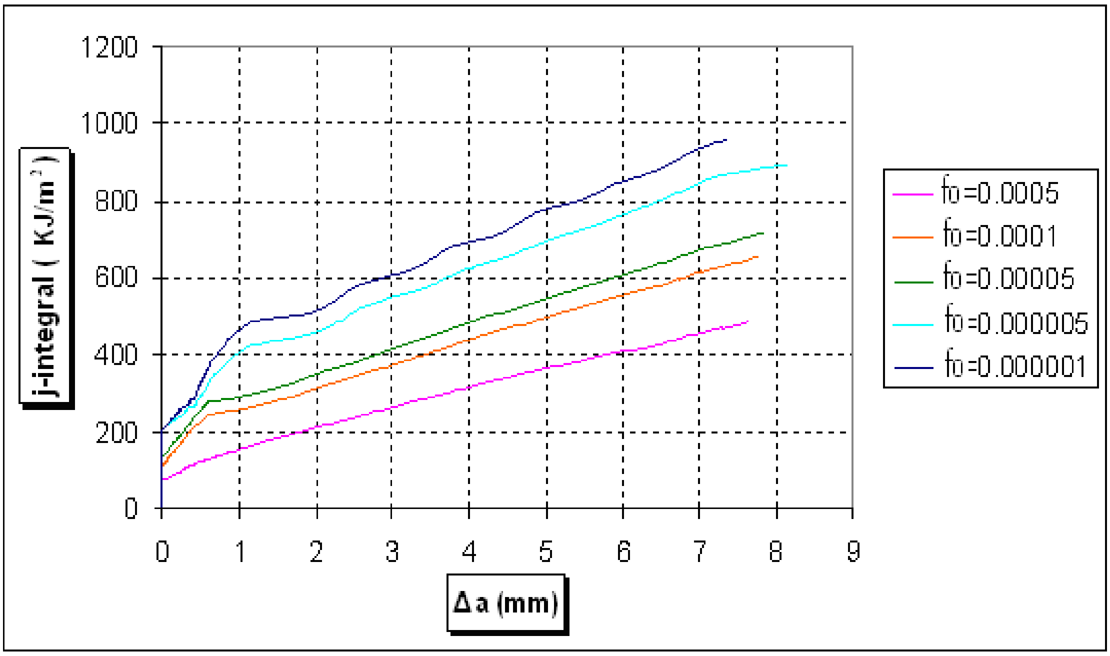

Figure 6.2 J-R curves for different f_o values

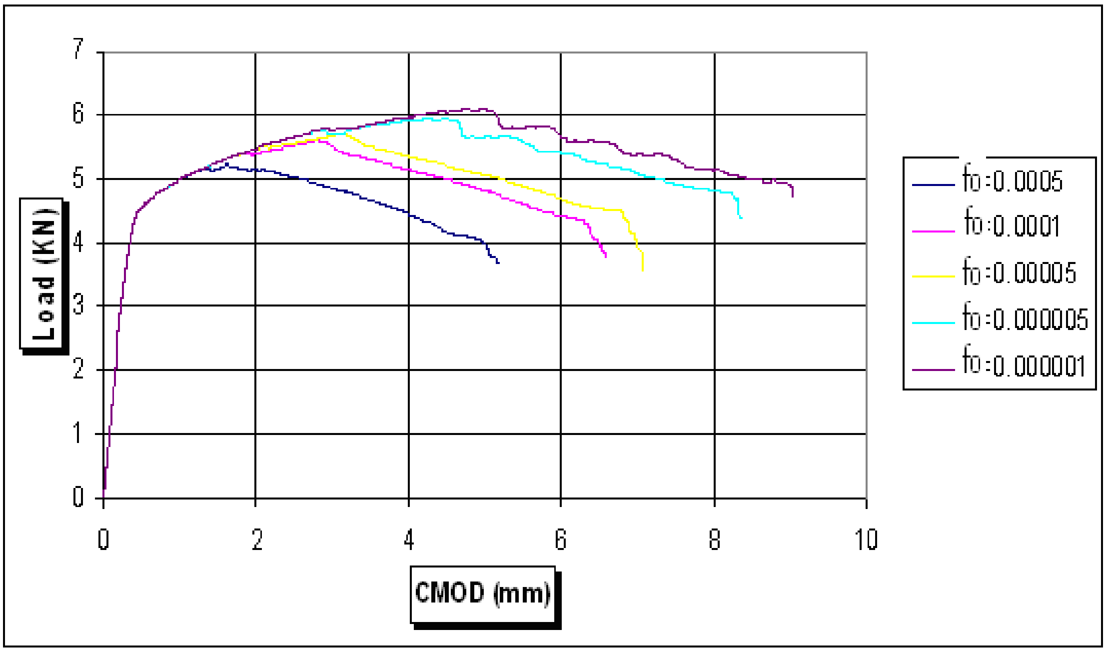

Figure 6.3 Load-CMOD curves for different f_o values

The variation of CMOD with Load is shown in figure 6.3. Load dropping point in load CMOD curve increases with decrease in f_o values

$\mathbf{f_o}$	**ΔD at sudden load drops (mm)**	**Slope Load-ΔD (KN/mm)**	**J_I (kJm^{-2})**
$f_o = 5x10^{-3}$	2.58	22.91	74.7149
$f_o = 1x10^{-3}$	2.70	20.90	114.1608
$f_o = 5x10^{-5}$	2.76	20.60	132.6453
$f_o = 5x10^{-6}$	2.76	20.60	200.1092
$f_o = 1x10^{-6}$	2.76	20.60	201.8662

Table 6.2 Effect of f_o on ΔD (at sudden load drop), Slope Load-ΔD and J_I (Initiation)

6.3 EFFECT OF CRITICAL VOID VOLUME FRACTION (F_C)

The Critical void volume fraction (f_c) is the critical value of void volume fraction at which the material stress carrying capacity starts to decay more rapidly due to void coalescence. Lower f_c means that the material reaches this point earlier. The load dropping point in the load – diametrical contraction curve is mainly influenced by this parameter. The J-R curves (Figure 6.5) shows that J_I is significantly affected by the critical void volume fraction. The J_i is affected almost linearly. Figure 6.6 shows the load versus CMOD curves for different values of f_c . Load dropping point is not much affected by f_c. There is slight decrease in its value with decrease in value of f_c.

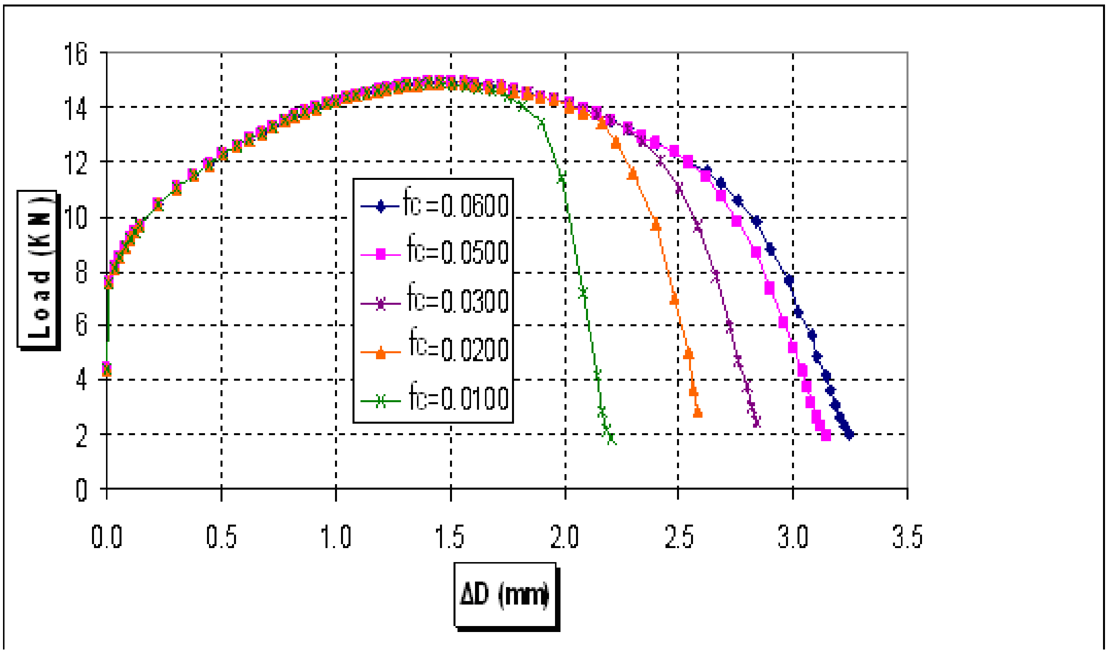

Figure 6.4 Load-ΔD curves for different f_c values

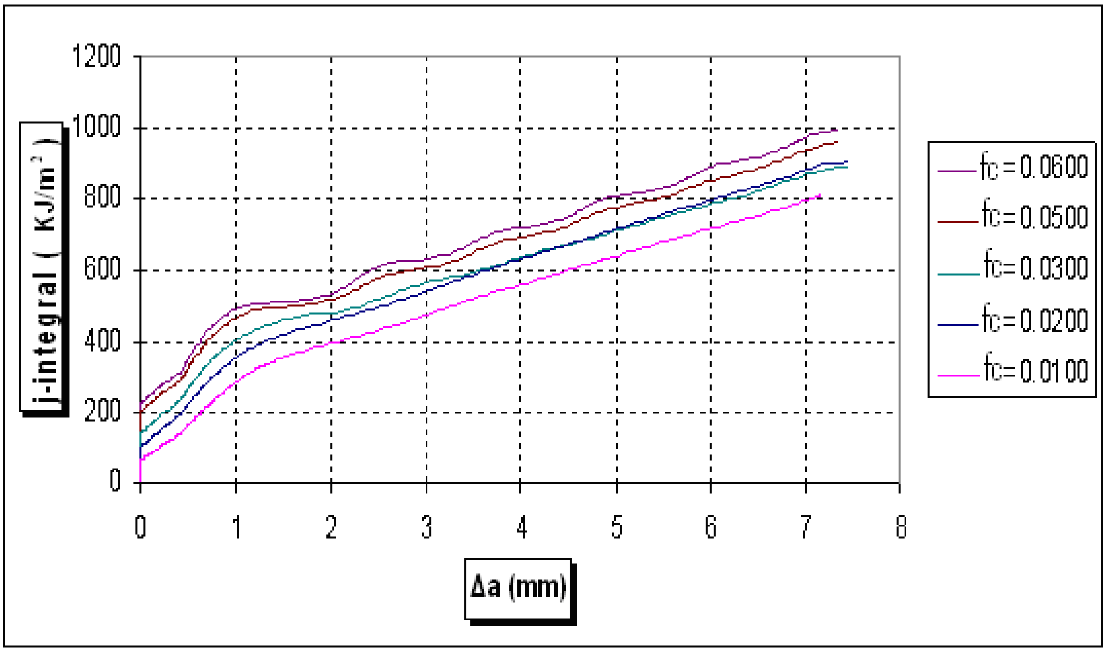

Figure 6.5 J-R curves for different f_c value

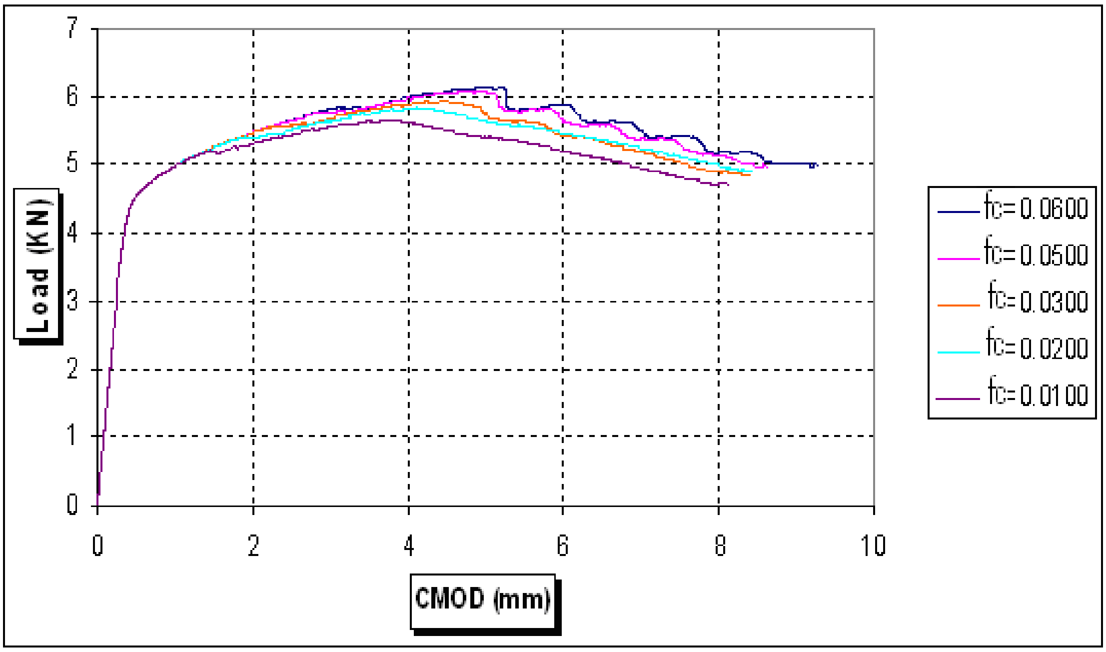

Figure 6.6 load-CMOD curves for different f_c value

f_c	ΔD at sudden load drops (mm)	Slope Load-ΔD (KN/mm)	J_I (kJm^{-2})
f_c =0.0600	2.84	19.49	225.2645
f_c =0.0500	2.76	20.60	201.8662
f_c =0.0300	2.58	27.72	139.1544
f_c =0.0200	2.40	38.22	100.6824
f_c =0.0100	1.98	46.51	64.0268

Table 6.3 Effect of f_c on ΔD (at sudden load drop), Slope Load-ΔD and J_I (Initiation)

6.4 EFFECT OF FINAL VOID VOLUME FRACTION (F_F)

Final void volume fraction (f_f) is the actual void volume fraction associated with the complete loss of stress carrying capacity of the material matrix. Lower values of f_f force the material to loss the stress carrying capacity earlier and thus a steeper slope is obtained (Figure 6.7). The load dropping point remains unaffected by f_f, while the slope varies linearly. The J_i is linearly affected by the final void volume fraction.

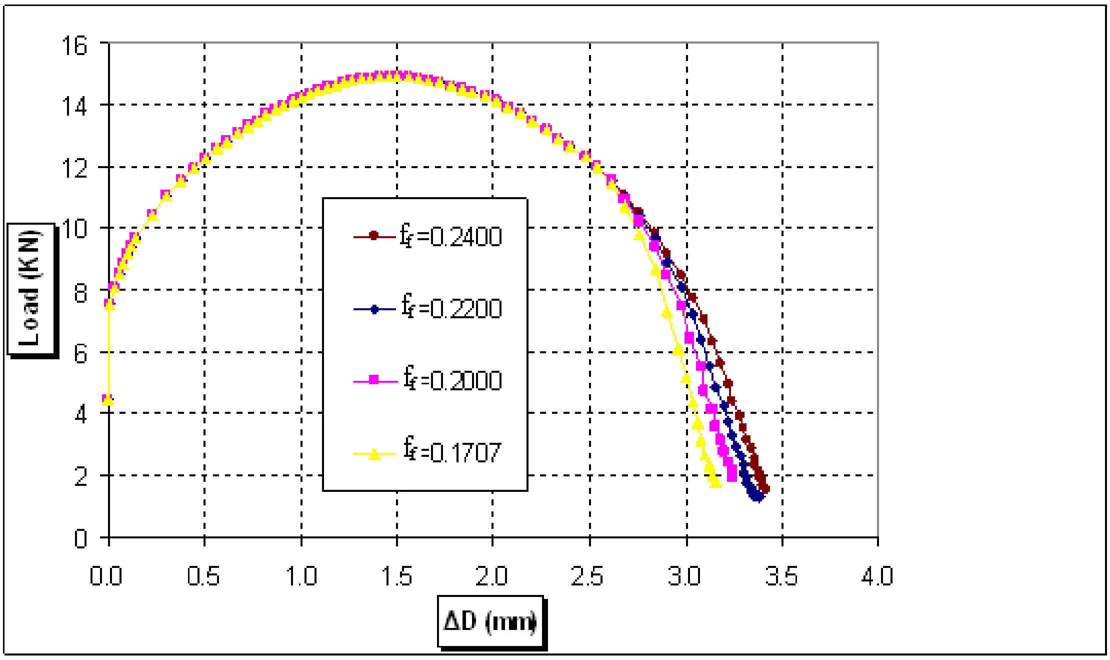

Figure 6.7 Load-ΔD curves for different f_f values

Figure 6.9 shows the load vs. CMOD curves for different values of f_f. Load dropping point is not affected by change in value of f_f.

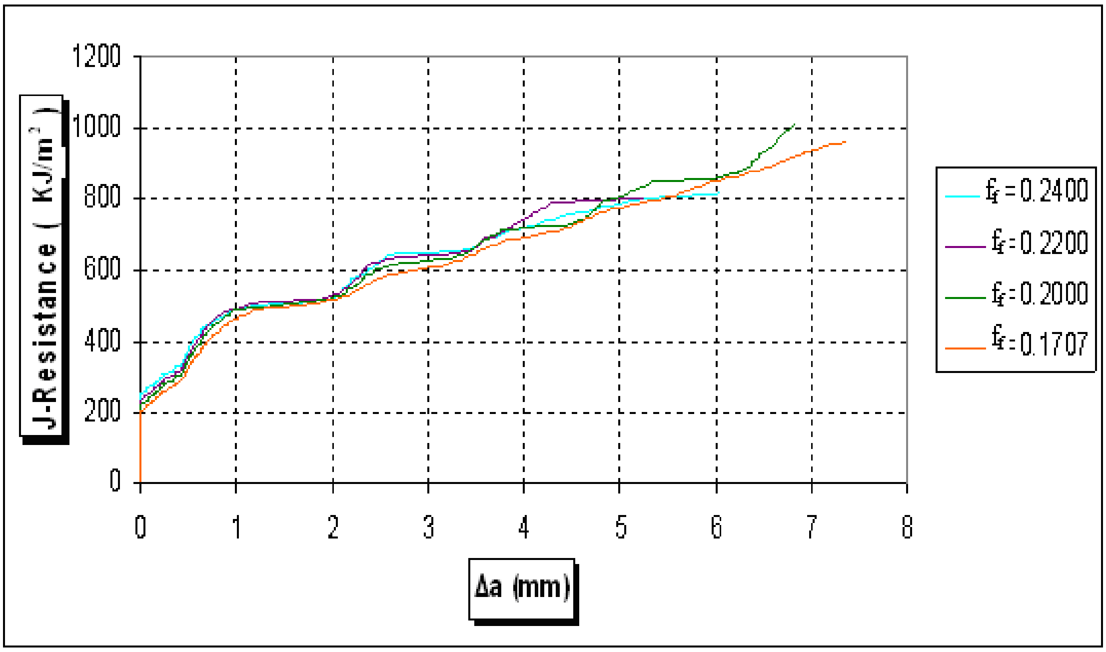

Figure 6.8 J-R curves for different f_f values

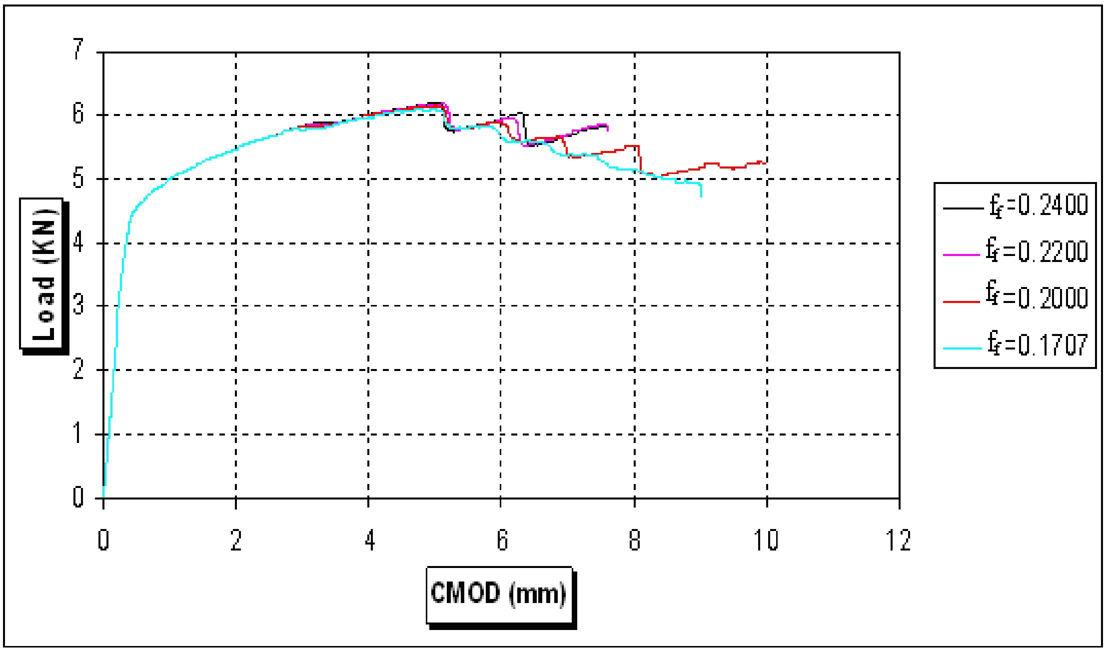

6.9 Load-CMOD curves for different f_f values

f_f	ΔD at sudden load drops (mm)	Slope Load-ΔD (KN/mm)	J_I (kJm^{-2})
f_f=0.2400	3.04	16.94	248.9091
f_f=0.2200	2.98	17.94	231.6716
f_f=0.2000	2.84	18.73	218.8738
f_f=0.1707	2.76	20.60	201.8662

Table 6.4 Effect of f_f on ΔD (at sudden load drop), Slope Load-ΔD and J_I (initiation)

6.5 EFFECT OF MEAN STRAIN OF VOID NUCLEATION (E_N):

It is determined by conducting tensile tests & subsequent metallographic examination. The Figure 6.10 clearly shows the effect of mean strain of void nucleation on load dropping point for notched tensile specimens. With increase in values of ε_n there is decrease in slope of load- ΔD curve. The effect of ε_n is more prominent in J-R curve as shown in Figure 6.11 .The study reveals that the J-initiation increases with increase in ε_n and the slope changes significantly with changing this parameter. Table 6.5 gives the ΔD (at sudden load drop), Slope Load-ΔD and Ji (initiation) for different values of ε_n

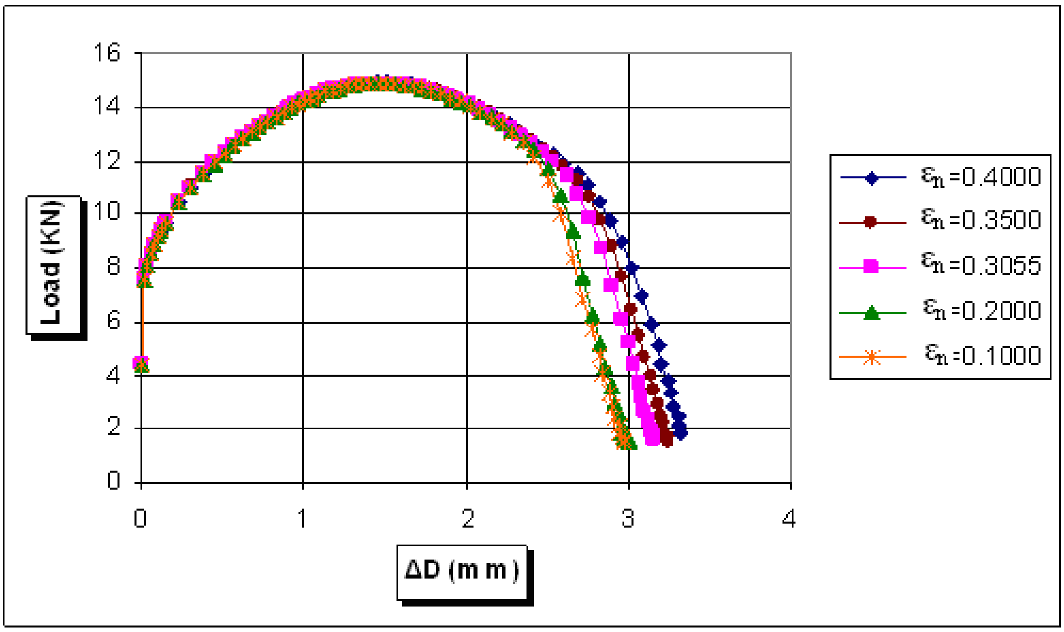

Figure 6.10 Load-ΔD curves for different ε_n values

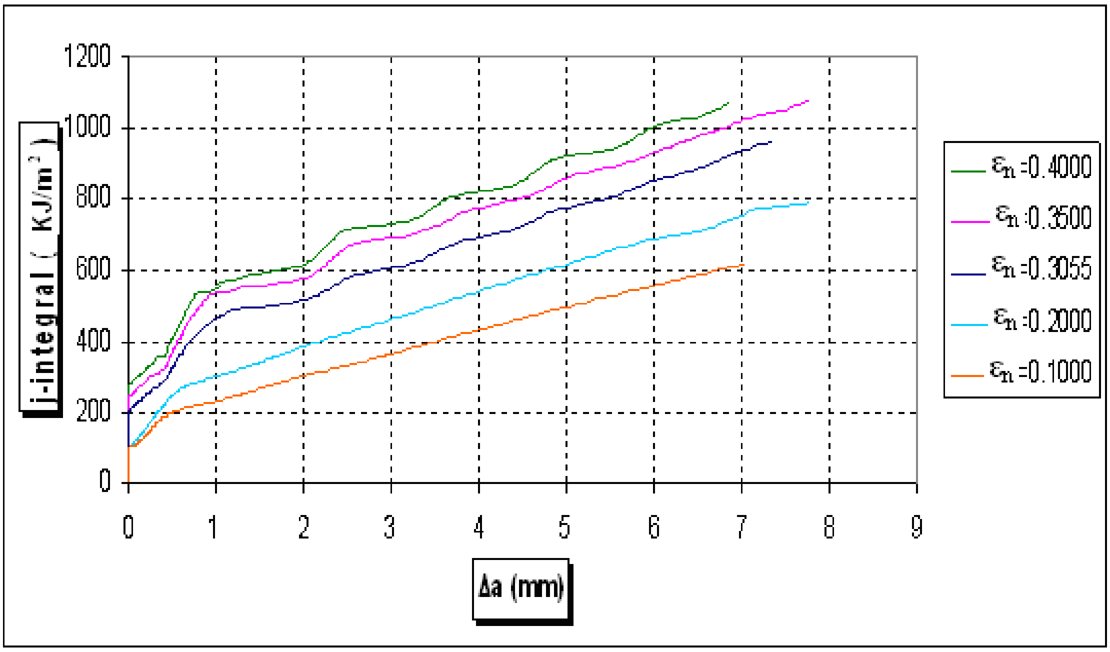

Figure 6.11 J-R curves for different ε_n values

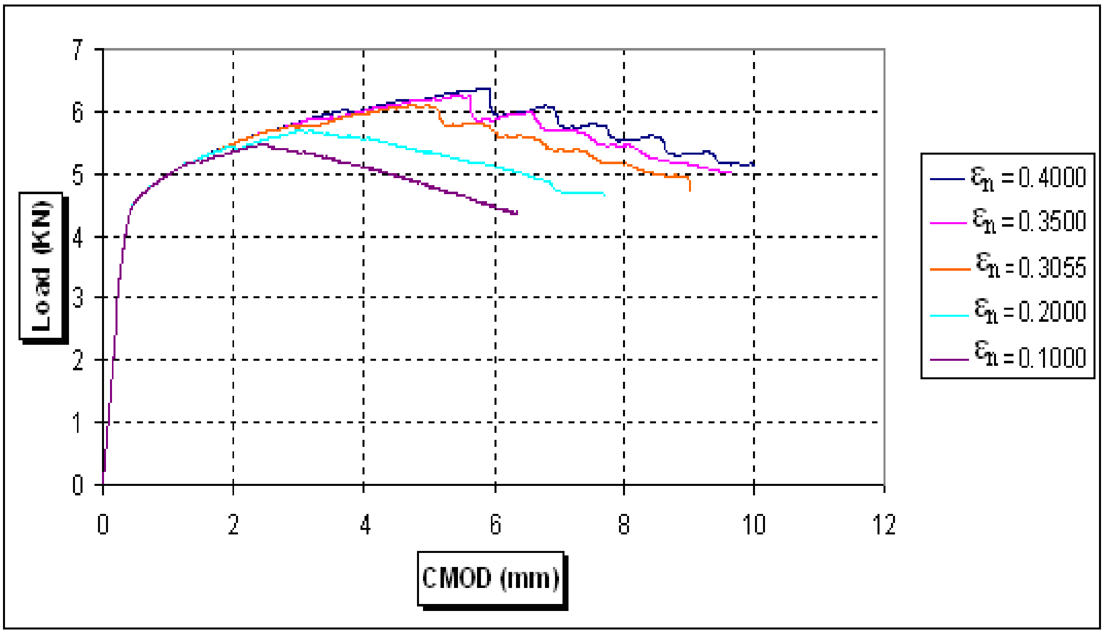

Figure 6.12 Load-CMOD curves for different ε_n values

Figure 6.12 shows variation of load vs. CMOD for different values of $\varepsilon_{n.}$ Load dropping point decreases with decrease in value of $\varepsilon_{n.}$

$\boldsymbol{\varepsilon_n}$	**ΔD at sudden load drops (mm)**	**Slope Load-ΔD (KN/mm)**	$\mathbf{J}_I$ **(kJm^{-2})**
ε_n =0.4000	2.96	19.6	275.0220
ε_n =0.3500	2.90	20.3	240.2838
ε_n =0.3055	2.76	20.6	201.8662
ε_n =0.2000	2.66	23.3	103.4713
ε_n =0.1000	2.58	24.8	101.2264

Table 6.5 Effect of ε_n on ΔD (at sudden load drop), Slope Load-ΔD and Ji (initiation)

6.6 EFFECT OF STANDARD DEVIATION OF NUCLEATION STRAIN 'S_N':

The process of nucleation follows statistical distribution. Chu & Needleman suggested a Gaussian distribution for the instantaneous volume fraction of nucleated voids with different values of strain. ε_N represents mean strain of this nucleation & S_N represents the standard deviation of nucleation strain. S_N is assumed generally as 0.1 for steel. It represents the scatter of nucleation strain. It can be determined from metallographic study of nucleation process of voids & finding the statistical distribution. The Figure 6.13 clearly shows the effect of standard deviation of nucleation strain on load dropping point for notched tensile specimens. With increase in values of S_n there is decrease in slope of load- ΔD curve. The effect of S_n on J-R curve as shown in Figure 6.14. The study reveals that the J-initiation does not changes significantly with change in S_n. Table 6.9 gives the ΔD (at sudden load drop), Slope Load-ΔD and Ji (initiation) for different values of S_n

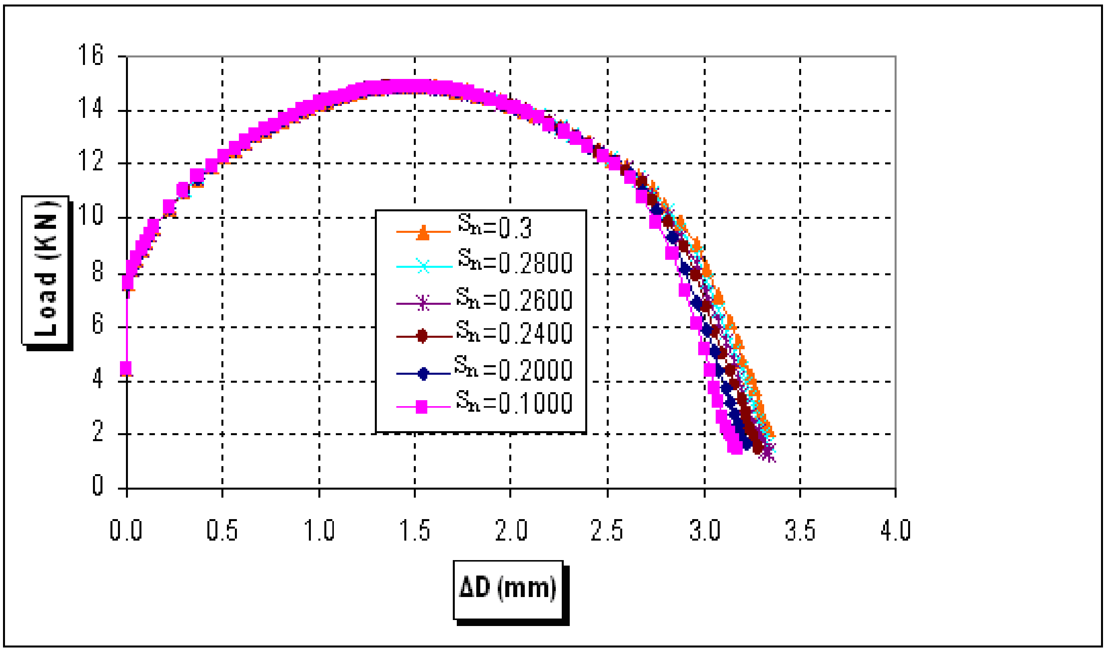

Figure 6.13 Load-ΔD curves for different S_n values

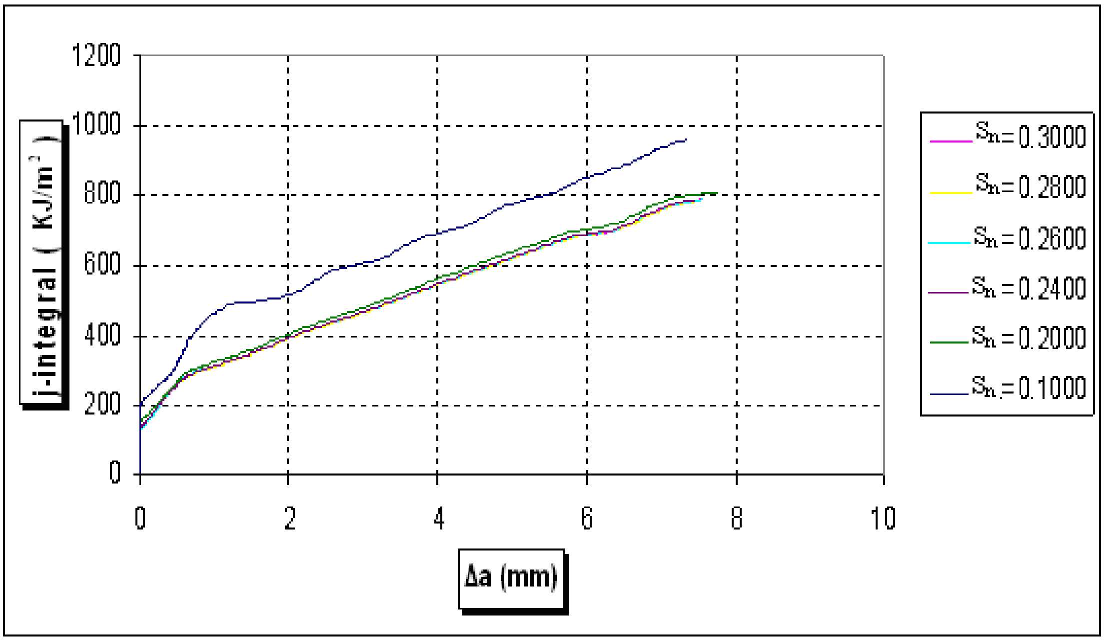

Figure 6.14 J-R curves for different S_n values

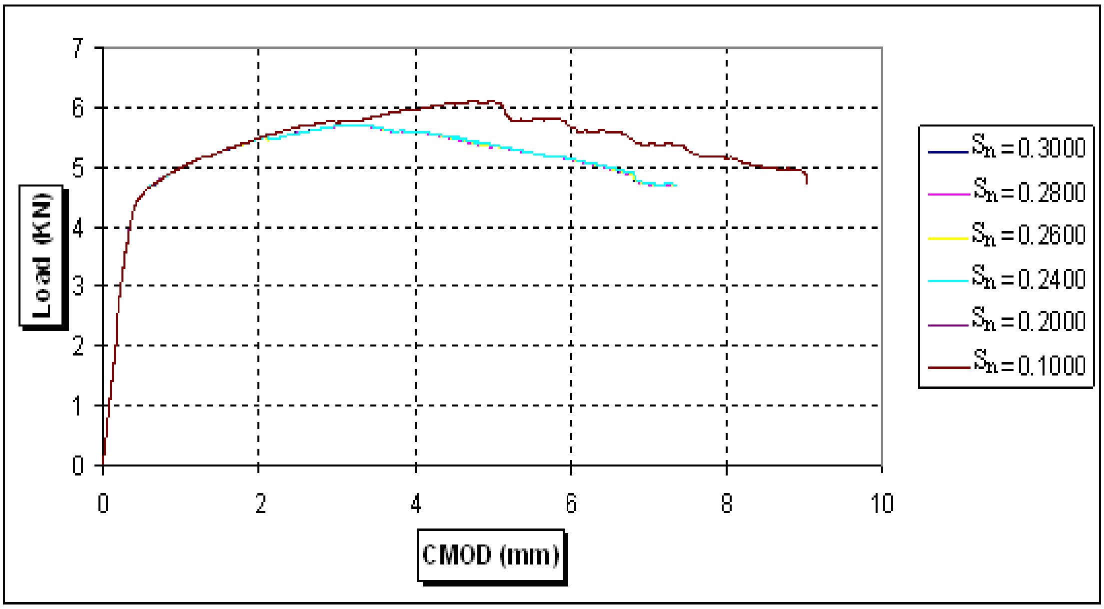

Figure 6.15 load-CMOD curves for different S_n values

Load dropping point is almost same for particular variation of S_n values. With further increase in value of S_n the load dropping point increases.

s_n	ΔD at sudden load drops (mm)	Slope Load-ΔD (KN/mm)	J_I (kJm^{-2})
s_n =0.3000	2.96	17.97	133.0752
s_n =0.2800	2.96	18.87	133.3193
s_n =0.2600	2.96	19.03	133.7225
s_n =0.2400	2.90	19.64	134.7301
s_n =0.2000	2.84	20.30	153.8188
s_n =0.1000	2.76	20.6	201.8662

Table 6.6 Effect of S_n on ΔD (at sudden load drop), Slope Load-ΔD and J_I (Initiation)

6.7 EFFECT OF VOID VOLUME FRACTION AT SATURATED NUCLEATION, 'F_N'

Effect of void volume fraction at saturated nucleation is shown in Figure 6.16 & 6.17. Overall effect of f_N on ΔD (at sudden load drop), Slope Load-ΔD and $\mathbf{J}_I$ (Initiation) is given in Table 6.7. Slope of Load- ΔD curve increases with increase in value of f_N and load dropping point decreases slightly, while Ji decreases with increase in f_N value.

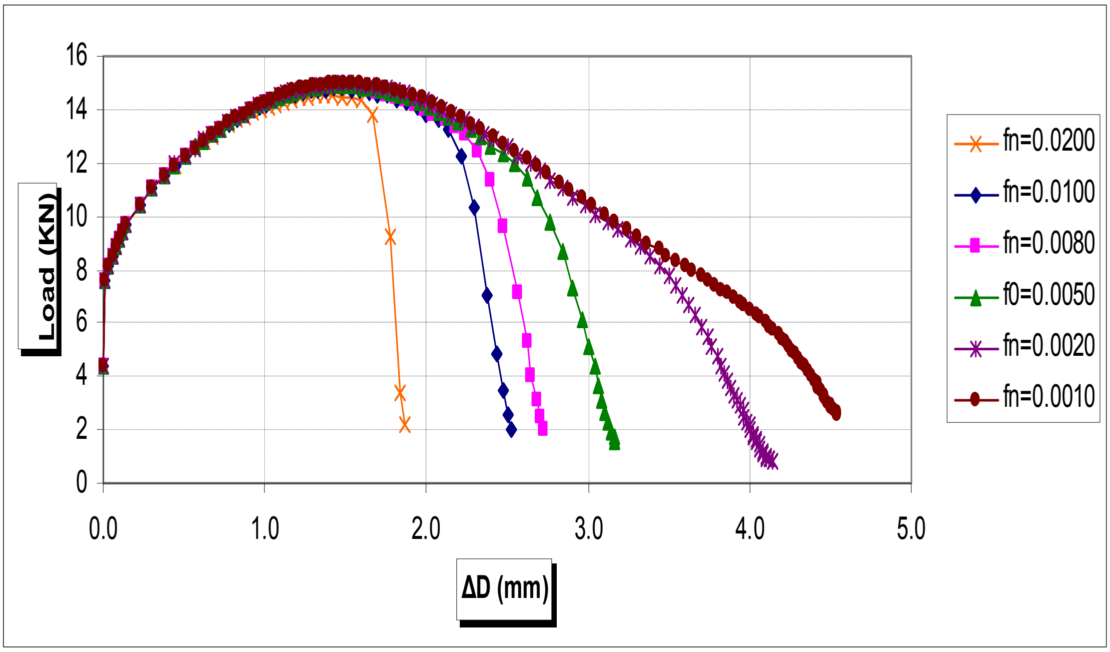

Figure 6.16 Load-ΔD curves for different f_n values

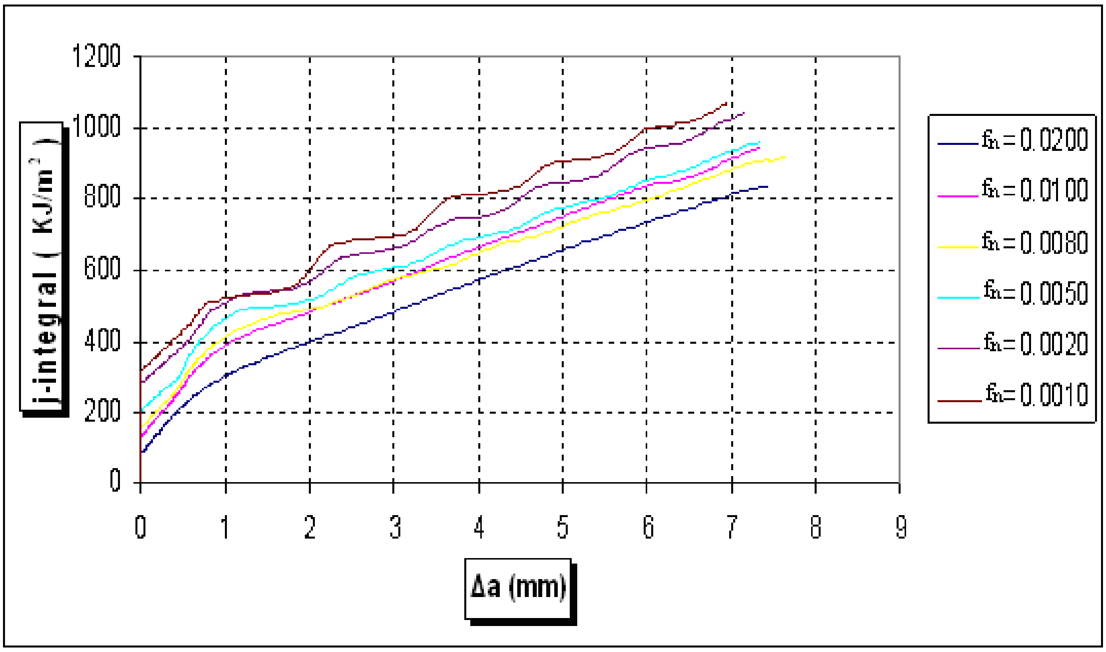

Figure 6.17 J-R curves for different f_n values

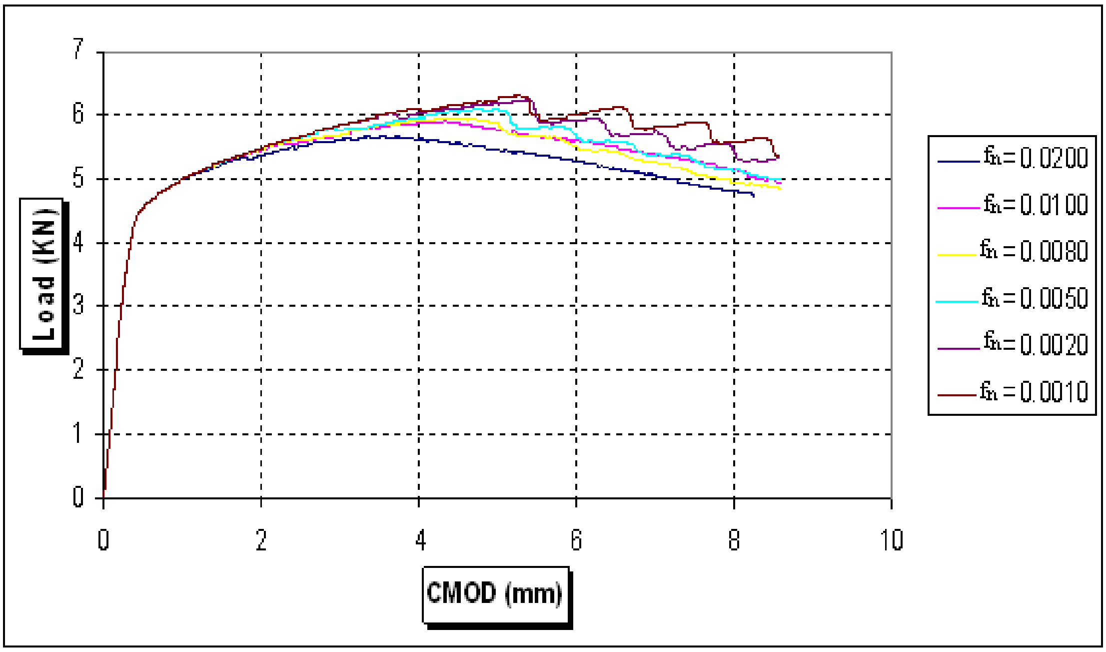

Figure 6.18 Load-CMOD curves for different f_n values

Load dropping point decreases with decrease in values of f_n. It can be seen in the figure above.

f_n	ΔD at sudden load drops (mm)	Slope Load-ΔD (KN/mm)	J_I (kJm^{-2})
f_n =0.0200	1.67	59.95	87.8192
f_n =0.0100	2.30	37.50	130.1785
f_n =0.0080	2.48	31.57	151.8157
f_n =0.0050	2.76	20.60	201.8662
f_n =0.0020	3.44	10.93	283.8112
f_n =0.0010	4.06	7.60	319.2932

Table 6.7 Effect of f_n on ΔD (at sudden load drop), Slope Load-ΔD and J_I (initiation)

6.8 DETERMINATION OF DAMAGE PARAMETERS FROM EXPERIMENTAL AND ANALYTICAL LOAD- ΔD CURVES

Effect of various damage parameters on Load-ΔD curve was studied in previous sections. Now the Gurson parameters for the nuclear steel are to be found using experimental and analytical load- ΔD curves of RNTS R2 & R4 by curve fitting of analytical curve to experimental curve by varying Gurson parameters.

6.8.1 Curve fitting of RNTS R2

The experimental and analytical load- ΔD curves for different values of Gurson parameters are shown in following Figure 6.19, 6.20.

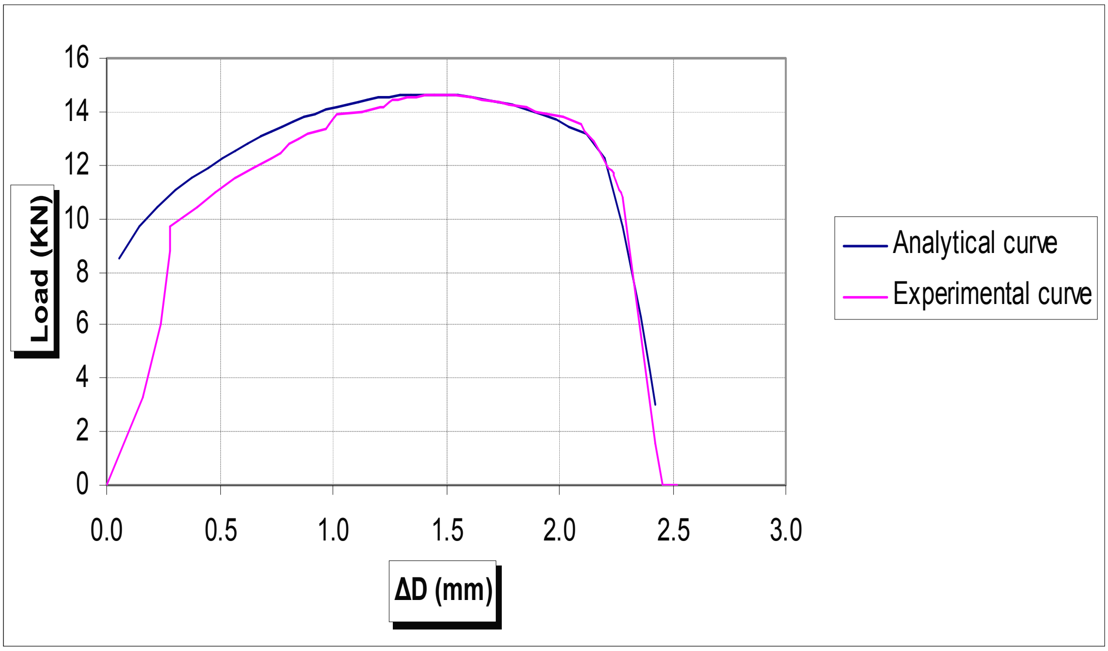

Figure 6.19 Experimental and Analytical load- ΔD curves for RNTS R2

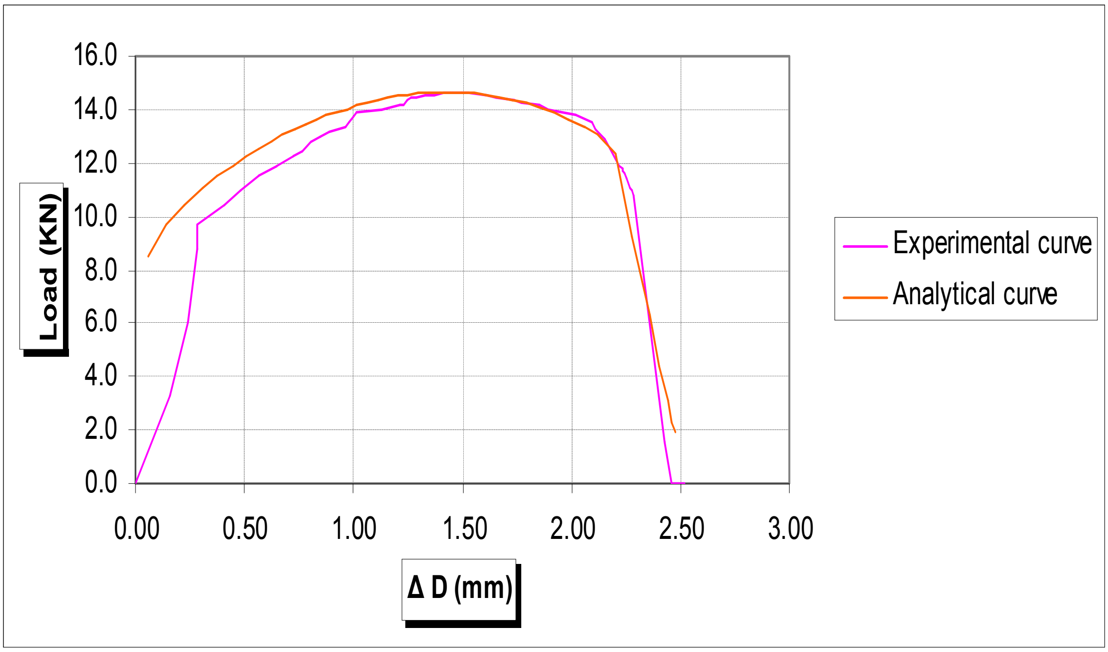

Figure 6.20 Experimental and Analytical load- ΔD curves for RNTS R2

Experimental load versus diametrical contraction curve match analytical curve for 2 set of gurson parameters. Table below show the value of all gurson parameters for these two set.

Gurson parameters	**Set 1**	**Set 2**
Initial void volume fraction, ‘f_o’	0.000001	0.000800
Critical void volume fraction, ‘f_c’	0.0800	0.0900
Final void volume fraction, ‘f_f’	0.1707	0.1707
Void volume fraction at saturated nucleation, ‘f_N’	0.0140	0.0130
Mean value of strain for nucleation, ‘ε_N’	0.3055	0.3055
Standard deviation of strain for nucleation, ‘S_N’	0.1000	0.0700
‘q_1’ Modifying parameters ‘q_2’ ‘q_3’	1.5 1.0 2.25	1.5 1.0 2.25
Critical length parameters ‘l_c’	0.2	0.2
Modified ultimate void volume fraction ‘f_u’	0.566	0.566

Table 6.8 Set of Gurson parameters that best approximate material behaviour for R2

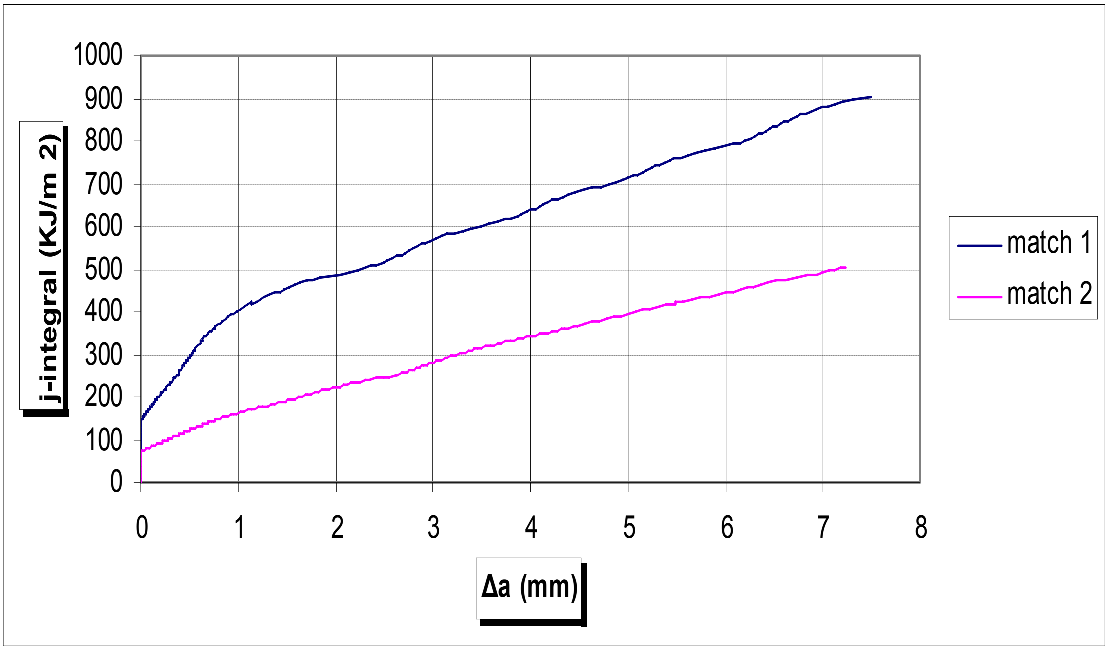

Figure 6.21 J-R curves for set 1 and set2

6.8.2 Curve fitting of RNTS R4

The experimental and analytical load- ΔD curves for different values of Gurson parameters are shown in following Figure 6.21.

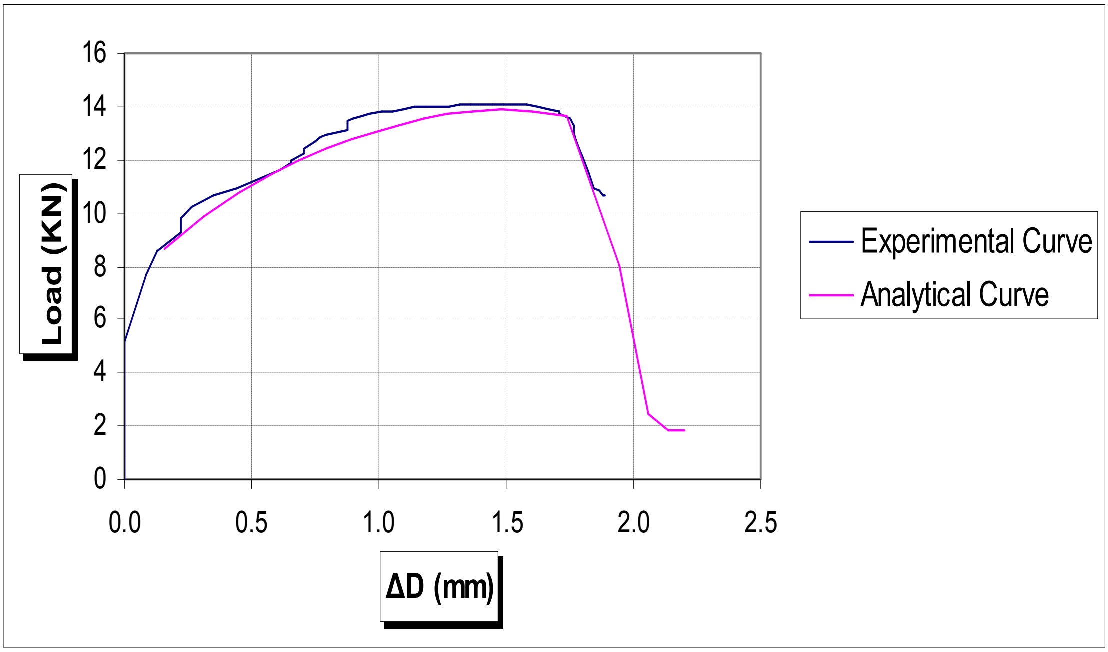

Figure 6.22 Experimental and Analytical load- ΔD curves for RNTS R4

We get one set of parameters those can best describe the material behaviour.

Gurson parameters	**Set 3**
Initial void volume fraction, 'f_o'	0.000001
Critical void volume fraction, 'f_c'	0.0500
Final void volume fraction, 'f_f'	0.1707
Void volume fraction at saturated nucleation, 'f_N'	0.0200
Mean value of strain for nucleation, 'ε_N'	0.3055
Standard deviation of strain for nucleation, 'S_N'	0.1000
Modifying parameters 'q_1' 'q_2' 'q_3'	1.5 1.0 2.25
Critical length parameters 'l_c'	0.2
Modified ultimate void volume fraction 'f_u'	0.566

Table 6.9 Set of Gurson parameters that best approximate material behaviour for R4

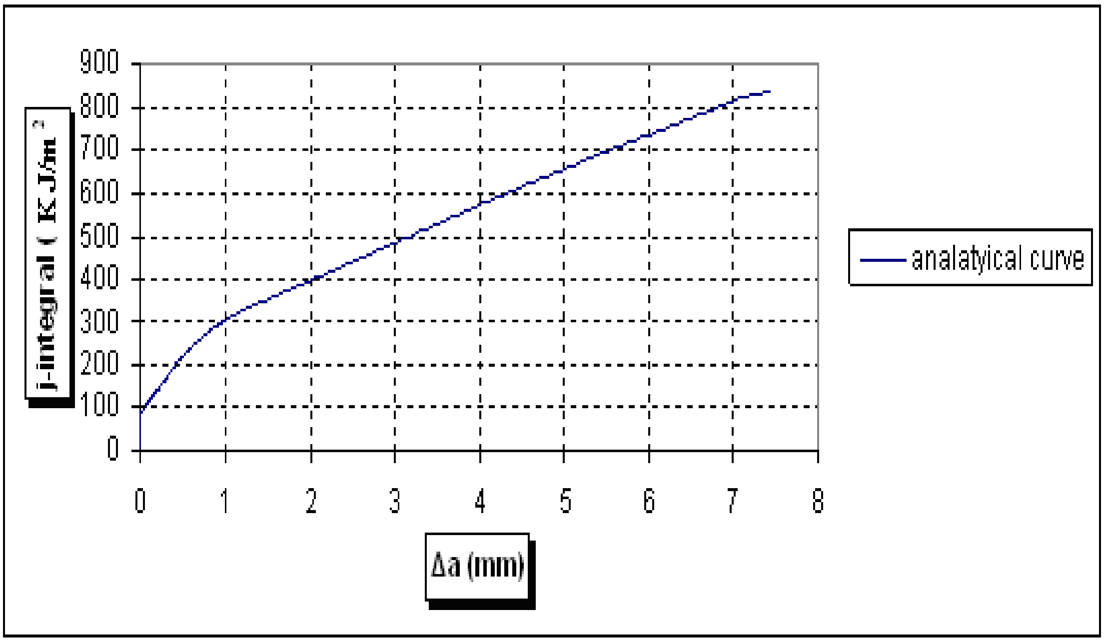

Figure 6.23 J-R curves for set 3

6.9 Comparison of experimental and analytical J-R curve:

For the three set of gurson parameters obtained J-R curves were plotted and compared with the experimental curve (obtained from BARC).

The figure 6.24 shows how the analytical J-R curve for the above 3 sets vary with experimental curve.

The set of gurson parameters for which the analytical curve matches the experimental curve are shown in table below.

	f_o	f_c	f_f	q_1	q_2	q_3	ε_N	S_N	f_N
Set 1	0.000001	0.0800	0.1707	1.5	1.0	2.25	0.3055	0.1000	0.0140

Table 6.10 Final set of Gurson parameters that best approximate material behaviour

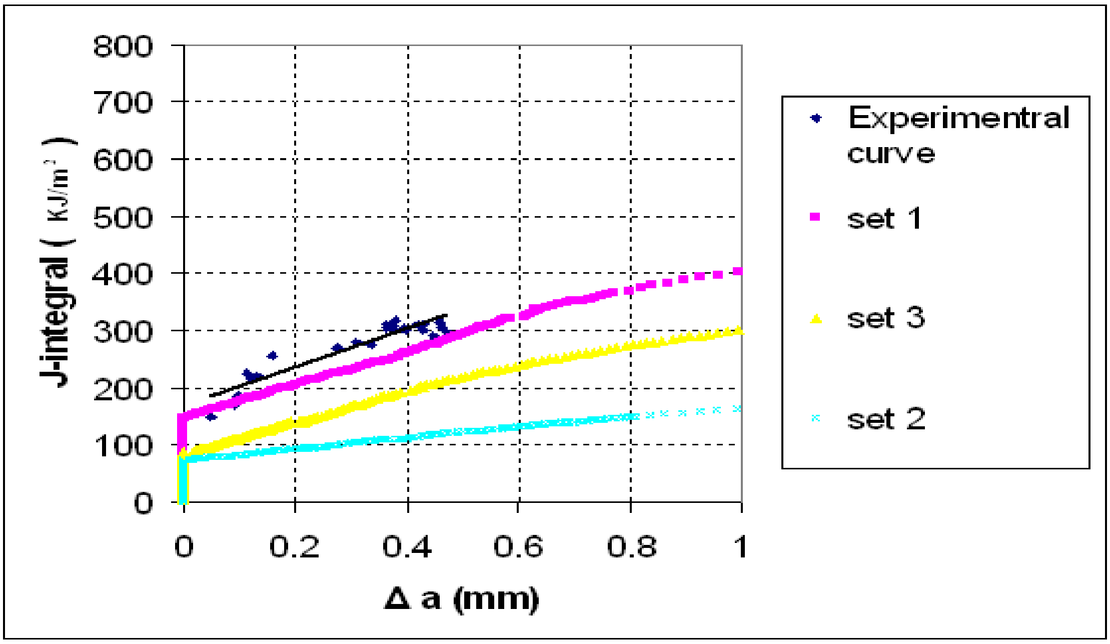

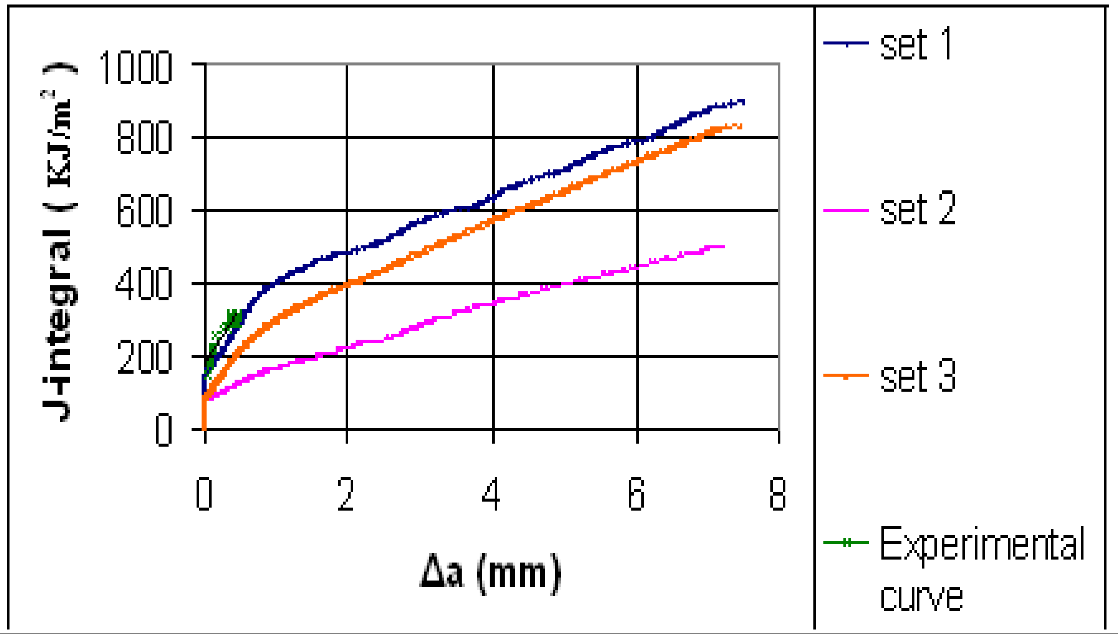

Figure 6.24 Experimental and Analytical J-R curves

CHAPTER 7

CLOSURE

1. CONCLUSIONS

From the present work following conclusions had been obtained

1. The following table presents an extraction of the study, i.e. how the gurson parameters affect the material behaviour. The four criteria being studied are the load dropping point and slope of the sudden drop of load in the load vs. diametrical contraction curve, the J-Initiation value and load dropping point in load-CMOD curve.

Gurson parameters	The load dropping Point in load- ΔD curve (RNTS specimen)	The final slope in load- ΔD curve (RNTS specimen)	$\mathbf{J}_I$ (CT specimen)	The load dropping Point in load-CMOD curve (CT specimen)
f_o	Yes	Slightly	Yes	Yes
f_c	Yes (parabolic)	Very much (parabolic)	Yes (linear)	Slightly
f_f	Yes	Yes (linear)	Slightly	Slightly
ε_N	Yes (linear)	Slightly	Yes	Yes
S_N	Slightly	Yes	Slightly	Slightly
f_N	Yes (linear)	Yes (linear)	Yes (linear)	Yes

Table 7.1 Effect of variation of gurson parameter on material behaviour

2. Curve fitting of analytical curve to experimental curve was done by varying the gurson parameters .The analytical curve matched the experimental curve for RNTS (R2) for 2 set of gurson parameters

The gurson parameters for RNTS (R2)

	f_o	f_c	f_f	q_1	q_2	q_3	ε_N	S_N	f_N
Set 1	0.000001	0.0800	0.1707	1.5	1.0	2.25	0.3055	0.1000	0.0140
Set 2	0.000800	0.0900	0.1707	1.5	1.0	2.25	0.3055	0.0700	0.0130

Table 7.2 Sets of Gurson parameters for which the analytical load- ΔD curve approximately matches the experimental curve for R2 (RNTS).

Guson parameters for RNTS (R4)

	f_o	f_c	f_f	q_1	q_2	q_3	ε_N	S_N	f_N
Set 3	0.000001	0.0500	0.1707	1.5	1.0	2.25	0.3055	0.1000	0.0200

Table 7.3 Set of Gurson parameters for which the analytical load- ΔD curve approximately matches the experimental curve for R4 (RNTS).

For these sets J-R curves were plotted and the analytical J-R curve approximates the experimental J-R curve for set 1. So the determined set of Gurson Parameters best describe the material damage behavior and can be used to model real life components of this material.

2. Guidelines for Future Work

1. The parameters ‘q1’,’q2’and ‘q3’ are not varied in the present work. They can also be varied and there effects can be observed. Currently to avoid complexity this has not been included.
2. The parameters determined from the present work may be checked on the different Specimen. In this case two properties are used (load vs. diametrical contraction and J-R curve). Similarly other properties may be used as per the experimental capability.
3. Current set obtained may be applied to other geometries and real time situation (at component level).
4. Size of mesh can be changed and there effects can be observed.

5. Similar studies can be done on lower and higher temperature effects.

REFERENCES

[1] J.R. Rice and D.M. Tracey. J. Mech. Phys. Solids 17 (1969), Pages. 201–217.

[2] A.S. Argon, J. Im and R. Safoglu. Metall. Trans. 6A (1975), pp. 825–837

[3] Gurson A.L. (1975) Plastic flow and fracture behavior of ductile materials incorporating void nucleation,

[4] Gurson A. L. (1977) Continuum theory of ductile rupture by void nucleation and growth: part I-yield

[5] Tvergaard V. (1981) Influence of voids on shear band instabilities under plane strain conditions. Int. J.

[6] Tvergaard V. (1982) on localization in ductile materials containing spherical voids. Znt. J. of Fract.

[7] Budiansky B, Hutchinson JW, Slutsky S. In: Hopkins HG, Sewell MJ, editors. Mechanics of solids—the Rodney Hill 60th anniversary volume. 1982. Pages. 13–45

[8] V. Tvergaard, A. Needleman, "Analysis of the cup-cone fracture in a round tensile bar ",Acta Metallurgica, Volume 32, Issue 1, January 1984, Pages 157-169

[9] W.H. Tai and B. Yang, Engng. Fract. Mech. **27** (1987), Pages. 371–378.

[10] G. Rousselier, Ductile fracture models and their potential in local approach of fracture. Nucl. Engng. Des. **105** (1987), Pages. 97–111.

[11] Dieter, G. E. (1988) Mechanical Metallurgy, MCGraw hill, 1988

[12] Clausmeyer, H., Kussmaul and K., Roos, E. "Influence of stress state on the failure behaviour of cracked components made of steel", ASME, Applied Mechanics Review, 44(2), 1991, Pages 77-92

[13] Schuler, X., Blind, D., Eisele, U., Herter, K.H. and Stoppler, W."Fracture Mechanics Evaluation of Cracked Components with Consideration of Multiaxility of Stress State", Nuclear Engineering Design, 1994, Pages 291-305

[14] J. Chattopadhyay, B.K. Dutta and H.S. Kushwaha, "Experimental and analytical study of three point bend specimen and through-wall circumferentially cracked straight pipe", Int. J. Pressure Vessels Piping 77 (2000), Pages 455–471.

[15] T.V. Pavankumar, J. Chattopadhyay, B.K. Dutta and H.S. Kushwaha, "Numerical investigations of crack tip constraint parameters in two dimensional geometries", Int. J. Pressure Vessels Piping 77 (2000), Pages 345–355

[16] Saini, s., "A New integral to quantify Damage Potential", M-Tech. thesis, IIT Roorkee.

[17] G. Bernauer and W. Brocks, Micro-mechanical modelling of ductile damage and tearing—results of a European numerical round robin. Fatigue Fract. Engng. Mater. Struct. **25** (2002), Pages 363–384

[18] Dutta B. K., Kushwaha H. S.,"A modified damage potential to predict crack initiation: theory and experimental verification", Engineering Fracture Mechanics, Volume 71, Issue 2, January 2004, Pages 263-275

[19] Pavankumara T.V., Samala M.K., Chattopadhyaya J., Dutta B.K., Kushwahaa H.S., Roosb E.,*, Seidenfussc M.," Transferability of fracture parameters from specimens to component level", International Journal of Pressure Vessels and Piping, Volume 82, Issue 5, May 2005, Pages 386-399

[20] Dutta, B. K., Saini, S and Arora N., "Application of a modified damage potential to predict ductile crack initiation in welded pipes", International journal of pressure vessels and piping, November 2005, Pages 833-839

[21] Acharyya S. , Dhar S. "A complete GTN model for prediction of ductile failure of pipe", Journal of Materials Science , Volume 43, Number 6 , March, 2008, Pages 1897-1909

[22] Seidenfuss M. Untersuchungen zur beschreibung des versagensverhaltens mit hilfe von schadigungsmodellen am beispiel des werkstoffes 20 MnMoNi 5 5. PhD Thesis, MPA Stuttgart, Germany, 1992